Journal of Materials Chemistry A

ROYAL SOCIETY OF CHEMISTRY

REVIEW

View Article Online
View Journal | View Issue

Cite this: J. Mater. Chem. A, 2022, 10, 20707

Covalent organic framework supported palladium catalysts

Hadi Salemi, [a] Maarten Debruyne,[a] Veronique Van Speybroeck, [b] Pascal Van Der Voort, [c] Matthias D'hooghe [a] and Christian V. Stevens *[a]

Received 30th June 2022
Accepted 20th September 2022

DOI: 10.1039/d2ta05234b

rsc.li/materials-a

Covalent organic frameworks (COFs), as highly porous crystalline structures, are newly emerging materials designed with tuneable features. They have a high potential to be a host to immobilize metal catalysts. The unique property of these materials, such as their high surface area, oriented channels, and heteroatom enrichment, make them promising materials to improve some disadvantages of heterogeneous metal catalysts. In this review, the fabrication and application of Pd anchored COFs as one of the most critical transition-metal catalysts that play a crucial role in a wide range of reactions is summarized.

1 Introduction

Palladium-catalyzed reactions are a wide range of transformations that usually cannot be achieved by classical techniques. The palladium catalyst facilitates and drives the conversion of less active organic precursors under milder reaction conditions in preparing pharmaceuticals, agrochemicals, and advanced materials. Some of the essential Pd-catalyzed reactions developed during the last decades are C–C cross-couplings,[1] C–N cross-couplings,[2] oxidative additions,[3] hydrogenation reactions,[4] *etc.*

A wide variety of techniques have been developed to improve the catalytic activity of homogeneous palladium catalysts towards high reaction rates, turnover numbers, selectivities, and yields. Many excellent catalysts have been developed based on phosphine ligands,[5] N-heterocyclic carbenes,[6] amines, dibenzylideneacetone (dba), *etc.* Even though homogeneous catalysts have proven their enormous relevance, there are some significant drawbacks are still present. The lack of reusability and catalysts residues contamination in end products is the main challenge of this group of catalysts.[1]

Heterogenization of catalysts by immobilizing of homogeneous catalysts on solid supports is one of the main methods to address these problems. Commercially available Pd/C and Pd/Al_2O_3 could be alternatives to homogeneous Pd catalysts, but the leaching of palladium, aggregation, and low efficacy makes them less suitable in many cases. Moreover, heterogeneous catalysts need harsher reaction conditions in comparison to homogeneous catalysts.[7]

Many new solid-supported palladium catalysts were designed during the last decades based on activated carbon,[8] inorganic oxides,[9,10] metal–organic frameworks (MOFs),[11] silica,[12] and porous organic polymers (POPs),[13,14] *etc.* to improve the catalytic activity and stability of Pd. An efficient solid-supported metal catalyst possesses a uniform dispersion of metals, such as palladium, and prevents its aggregation. Therefore, the support often possesses chelating groups such as phosphine ligands and amine groups or incorporate heteroatoms such as nitrogen, sulfur, and phosphorous, which improve the chemical and electrical properties of the substrate and its interaction with metal catalysts. Although functionalization and heteroatom doping are efficient methods, they still require extra synthetic steps.

Covalent organic frameworks (COFs)[15] are porous, crystalline, lightweight polymers ingeniously constructed by strong covalent bonds between light elements (H, B, C, N, and O). The high surface area and accompanying porosity, tuneable pore size, and well-ordered channels of these materials make them a promising choice for a wide range of applications such as gas storage,[16,17] optoelectronics,[18] photocatalysis,[19] electro-activated catalysis,[20] semiconductive and photoconductive devices.[21]

To achieve crystalline materials, such as COFs, error correction during the synthesis is needed, and thus reversible reactions and carefully fine-tuned reaction procedures are used. The most commonly applied reactions to synthesize COFs are boronic acid trimerization, boronate ester formation, the trimerization of nitriles, and Schiff base condensation.[22]

Due to the strong covalent bonds, the abundance of heteroatoms, and the possibility for highly tuneable structures, COFs are highly promising materials for the immobilization of metals. The main important factors that should be considered for COFs as solid support are their thermal stability and resistance in aqueous acidic and basic solvents. In contrast to the hydrolytically unstable boroxine or boronate-ester COFs,

[a]Department of Green Chemistry and Technology, Ghent University, Campus Coupure, Coupure Links 653, 9000 Gent, Belgium. E-mail: Chris.Stevens@UGent.be
[b]Department of Chemistry, Ghent University, Krijgslaan 281 (S3), 9000 Ghent, Belgium
[c]Department of Applied Physics, Ghent University, Technologiepark 46, 9052 Zwijnaarde, Belgium

triazole-, imine-, and hydrazone-based COFs are appropriate materials for this application.

Herein, synthesis and application of Pd/COF hybrids in catalytic reactions are covered. Also, some important characteristics of the prepared structures, such as surface area, Pd nanoparticles (NPs) size, and palladium loading are discussed. In this review, the Pd/COFs are classified into six categories based on the structure of the COFs that are used for immobilization of the palladium: (1) COF-LZU1, (2) COF-TpPa, (3) triazine-based COFs, (4) functionalized COFs, (5) other 2D-COFs, (6) 3D-COFs. Finally, the efficiency of the prepared Pd/COFs is compared in the Suzuki–Miyaura coupling reaction as the most commonly explored reaction.

2 Synthesis and application of Pd/COF catalysts

2.1 COF-LZU1

The imine-linked COF-LZU1 was synthesized for the first time by Wang and co-workers through condensation of 1,3,5-triformylbenzene and 1,4-diaminobenzene under solvothermal conditions (Table 2, entry 1). The prepared precipitates are insoluble in water and common organic solvents and morphological studies proved an eclipsed layered-sheet arrangement for the COF-LZU1 stabilized by π–π stacking interaction between adjacent layers. Porosity studies of COF-LZU1 showed 410 $m^2 g^{-1}$ surface area and 0.54 $cm^3 g^{-1}$ pore volume (Fig. 1).[23]

The preparation of the first Pd/COF hybrid (Pd/COF-LZU1) was reported by treating the COF-LUZ1 with $Pd(OAc)_2$. Characterization of the catalyst by ^{13}C chemical shift and the binding energy (BE) of $Pd_{3d5/2}$ proved the existence of palladium in the +2 oxidation state stabilized between the layers of the COF by coordination with the nitrogens of the imines. Moreover, the prepared catalyst showed a significantly reduced pore volume and surface area of 0.19 $cm^3 g^{-1}$ and 146 $m^2 g^{-1}$, respectively. The catalytic activity of Pd/COF-LZU1 in the Suzuki–Miyaura coupling reaction showed a high yield in *p*-xylene at 150 °C (Table 1, entry 1). The material could be recycled four times without losing activity, proving the high stability for this catalyst under harsh reaction conditions.

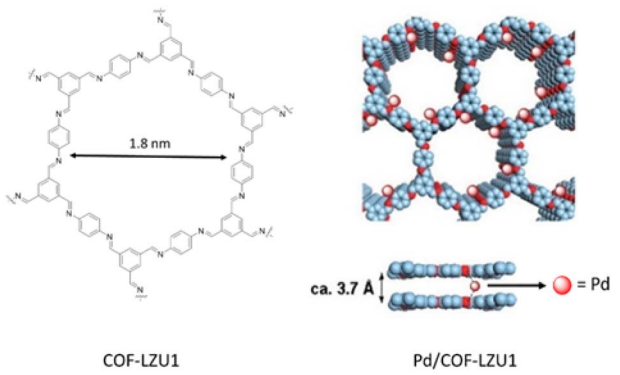

Fig. 1 Construction of COF-LZU1 and Pd/COF-LZU1 (reproduced from ref. Ding *et al., J. Am. Chem. Soc.*, 2011, **133**, 19816–19822 copyright 2011 American Chemical Society).

In further research, the pyrolysis of Pd/COF-LZU1 gave rise to N-doped hollow carbon spheres (NHCS) containing Pd NPs (Fig. 2). The NHCS possessed a diameter and thickness of 200 nm and 30 nm, respectively, and surface areas of 450–550 $m^2 g^{-1}$. The Pd nanoparticles possess an average size of 6 nm, and are uniformly dispersed at the carbon shell. The final catalyst included 2.4 wt% Pd and 11.0 wt% nitrogen (Table 2, entry 2).[24]

The catalytic activity of Pd@NHCS was explored by the hydrogenation reaction of nitrobenzene to aniline under atmospheric pressure of H_2 at 25 °C. This metal-hybrid catalyst showed much better catalytic activity and selectivity relative to $Pd(OAc)_2$ and was recyclable at least five times without significant loss of catalytic activity and selectivity.

Kim and co-workers designed and synthesized a metal-doped core–shell structure by combining metal organic frameworks (MOFs) and COFs as a new green platform for photocatalysis (Fig. 3) (Table 2, entry 3). TiATA MOF was used as a core which was coated with LZU1 COF to prepare TiATA@LZU1. Pd nanoparticles were then immobilized *via* coordination of $Pd(OAc)_2$ followed by reduction to give rise to the metal-doped core–shell structure Pd/TiATA@LZU1.[25]

The XRD pattern of TiATA@LZU1 was similar to the previously reported XRD of TiATA with the inclusion of some signals corresponding to the LZU1 pattern. Also, morphological studies with SEM and TEM showed the expected core–shell structure that palladium nanoparticles that were uniformly dispersed on the 2D COF shell with an average size of 2.2 nm.

The photocatalytic activity of Pd/TiATA@LZU1 was evaluated by the selectively hydrogenation of the olefin group of styrene under visible light irradiation. Styrene was completely converted with high selectivity to ethylbenzene in 15 minutes using hydrogen gas. Moreover, *in situ* hydrogen generation by dehydrogenation of ammonia to hydrogen was possible with excellent yield and selectivity in 68 seconds in a dual-chamber microreactor.

In 2020, Yu and co-workers designed a one-pot *in situ* method to synthesize a new nanocatalyst based on the encapsulation of Pd nanoparticles into the hollow polyamine spheres of covalent organic frameworks (Pd@H-PPA) (Table 2, entry 4). They prepared Pd@H-PPA by reducing the Pd^{2+} and imine linkages of Pd/COF-LZU1 to Pd nanoparticles and amine linkages (Fig. 4a). Morphological analysis indicated well-dispersed Pd nanoparticles with an average size of 2.6 nm in the structure of the H-PPA shell. The main advantage of this method is the confinement of palladium nanoparticles by amine functional groups during nucleation, causing small and narrowly distributed palladium nanoparticles.[26]

The catalytic activity of Pd@H-PPA was investigated in the hydrogenation of nitroarenes in the presence of ammonia borane (AB) as the hydrogen source. The authors found that this catalyst has excellent efficiency for this reaction under mild conditions (aqueous solution, 30 °C) and short reaction times. According to the suggested mechanism for this catalytic process, the ammonia group of ammonia borane (AB) could be replaced by the amine linkage of H-PPA to make a borane–H-PPA adduct. This process facilitates a hydrogen generation process and enhance the rate of the reduction of nitro groups (Fig. 4b).

Table 1 Application of Pd/COFs hybrids in the Suzuki–Miyaura cross-coupling reaction of bromobenzene and phenyl boronic acid

Entry	Catalyst	Oxidation state	Surface area ($m^2 g^{-1}$)	Solvent	Temperature (°C)	Time (h)	Yield (%)	Stability (runs)	Ref.
1	Pd/COF-LZU1	Pd^{2+}	146	*p*-Xylene	150	3	97	5	23
2	(Pd/C)@TpPa	Pd^0	166	EtOH/H_2O	30	24	87	5	33
3	Pd/TATAE	Pd^{2+}	104	H_2O	RT	2	98	4	40
4	Pd^{II}/TAT–DHBD	Pd^{2+}	139	DMF	120	24	56	—	41
5	Pd^0/TAT–DHBD	Pd^0	21.5	DMF	120	24	62	—	41
6	Pd^{II}/TAT–TFP	Pd^{2+}	292	DMF	120	24	80	5	41
7	Pd^0/TAT–TFP	Pd^0	52.2	DMF	120	24	83	5	41
8	Pd@COF-TM	Pd^{2+}	—	H_2O	RT	6	99	9	50
9	Pd@OC-MA	Pd^{2+}	8.6	H_2O	RT	5	99	4	52
10	PdNPs@Thio-COF	Pd^0	—	DMF/H_2O	50	3	85	5	54
11	Pd@COF-NHC	Pd^0	18.8	H_2O	RT	1	99	8	56
12	Pd@COF-QA	Pd^0	26	H_2O	50	6	99	10	58
13	TAPB–BTCA	Pd^0	494	THF	80	2	51	—	70
14	PdNPs@Phos-COF-1[a]	Pd^0	—	DMF/H_2O	50	2	>99	5	73
15	Pd/COF-SMC2	Pd^{2+}, Pd^0	24	EtOH	80	1	96	4	75
16	Pd/Phen-COF	Pd^{2+}	447	i-PrOH/H_2O	RT	16	99	5	76
17	Pd/H_2P-Bph-COF	Pd^{2+}	147	Toluene	110	1.5	98	5	60
18	$Pd(OAc)_2$@COF-300	Pd^{2+}	270	MeOH/H_2O	70	0.3	100	6	83
19	Pd(II)@SP-3D-COF-Bpy	Pd^{2+}	640	*p*-Xylene	70	2	98	5	84
20	Pd@TPM-3D-COF-Bpy	Pd^0	—	DMF/H_2O	70	5	98	5	85

[a] 4-Bromotoluene was used as reactant.

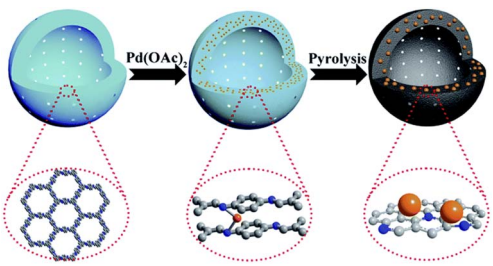

Fig. 2 Fabrication of Pd@NHCS. Color coding: grey, carbon; blue, nitrogen; orange, Pd precursors or NPs (reproduced from ref. Chen *et al.*, *Chem. Sci.*, 2016, **7**, 6015–6020 with permission from the Royal Society of Chemistry).

To alleviate the need for a catalyst separation step, the authors designed a reactor for the tandem reaction of dehydrogenation of AB and hydrogenation of nitroarenes. Although the reaction needs more time to complete in this way, it still works very efficiently.

Jia and co-workers studied the effect of acetic acid concentration in the one-pot synthesis of Pd@COF-LZU1. They used 0, 0.5, 1, 3, 6, and 17.5 mol L^{-1} acetic acid in water as the catalyst for COF formation and found that the particle sizes of COF-LZU1 decreased from 800 nm to 225 nm by increasing the acid concentration. In addition, the palladium content of Pd@COF-LZU1 is increased to 13.6% for 3 mol L^{-1}, which is much higher than the post-synthesis method with 4.32% Pd content. Also, the porosity study indicates a decrease from 517 $m^2 g^{-1}$ to 127 $m^2 g^{-1}$ for the surface area and from 1.66 $cm^3 g^{-1}$ to 0.49 $cm^3 g^{-1}$ for the pore size, respectively. By increasing the concentration of acetic acid, these amounts dropped, which is related to the higher rate of COFs formation.[27]

Pd@COF-LZU1 Possessed a 20 times higher rate constant than $Pd(OAc)_2$ for reducing 4-nitrophenol to 4-aminophenol in aqueous solution by $NaBH_4$. Also, the investigation demonstrates a good stability and reusability for the catalyst after five cycles, although the reaction time slowly increased from 6 minutes to 12 minutes.

Wang and co-workers designed a biosensor nanocomposite based on the COF-LZU1 to detect cancer cells (Table 2, entry 5). They encapsulated Pd nanoparticles in the carboxymethyl cellulose-modified covalent organic framework (CMC-COF-LZU1) hydrogel and functionalized it with folic acid (FA) as a cancer cell identifier. The folic acid group gives the FA–Pd NPs/CMC-COF-LZU1 the ability to target folate receptor (FR)-positive cancer cells. The BET analysis indicates 460 $m^2 g^{-1}$, 309 $m^2 g^{-1}$ and 402 $m^2 g^{-1}$ for COF-LZU1, CMC-COF-LZU1, and Pd NPs/CMC-COF-LZU1, respectively. TEM analysis indicated well dispersed Pd nanoparticles with an average size of 4 nm.[28]

The detection of cancer cells was explored by colorimetric and fluorescence emission of catalytic transformation of *N*-butyl-4-NHAlloc-1,8-naphthalimide (NNPH) into *N*-butyl-4-amido-1,8-naphthalimide (NPH) with a FA–Pd NPs/CMC-COF-LZU1 nanocomposite (Fig. 5).

2.2 COF-TpPa

TpPa-1 was reported in 2012 as the first reported β-ketoenamine-linked COF by the Schiff-base reaction and keto–enol tautomerization of 1,3,5-triformylphloroglucinol (Tp) with

Table 2 The summarized synthesis procedure of catalysts

Entry	COFs	Precursors[a]	Synthesis procedure	Ref.
1	Pd/COF-LZU1	TFB + PDA	- Dioxane/AcOH, 120 °C, 3 days - $Pd(OAc)_2$ solution in DCM	23
2	Pd@NHCS	TFB + PDA	- Dioxane/AcOH, 120 °C, 3 days - $Pd(OAc)_2$ solution in DCM - Carbonized at different temperatures	24
3	TiATA@LZU1	TiATA MOF, TFB + PDA	- Dioxane/AcOH, r.t., 3 days - $Pd(OAc)_2$ solution in DCM - $NaBH_4$	25
4	Pd@H-PPA	TFB + PDA	- Dioxane/AcOH, r.t., 4 days - $Pd(OAc)_2$ solution in DCM - THF : water (4 : 1), $NaBH_4$, 70 °C	26
5	Pd NPs/CMC-COF-LZU1	CMC-NH_2, TFB + PDA	- Dioxane/AcOH, 25 °C, 4 days - $Pd(OAc)_2$ solution in DCM : EtOH (1 : 1), reflux	28
6	Pd@TpPa-1	Tp + PDA	- Mesitylene/dioxane/AcOH, 120 °C, 3 days - Na_2PdCl_4 solution in MeOH, $NaBH_4$	30
7	Pd@H-TpPa	ZIF-8, Tp + PDA	- Coating ZIF-8 with an amorphous polyimine network - Acidic etching in a dioxane/aqueous acetic acid mixture	32
8	(Pd/C)@TpPa	(Pd/C)@SiO_2, Tp + PDA	- Mesitylene/dioxane/AcOH, 120 °C, 3 days	33
9	Pd@COF/NFC	NFC membrane, Tp + PDA	- Mesitylene/dioxane/AcOH, 120 °C, 3 days - $Pd(OAc)_2$ solution in EtOH; $NaBH_4$	35
10	Pd@COF-280	Tp + PDA	- Calcination Tp/PDA in the presence of PTSA (280 °C, 4 h) - $Pd(OAc)_2$ solution in MeOH	36
11	Pd@CCOF-MPC	Cyanuric chloride + *S*-2-methylpiperazine	- Anhydrous dioxane, 90 °C, 36 h - $Pd(NO_3)_2$ solution in MeOH	37
12	Pd(II)/COF-SDU1	TRIF + PDA	- *o*-Dichlorobenzene/*n*-butanol/AcOH, 85 °C, 7 days - $Pd(OAc)_2$ solution in DCM	38
13	Pd/TATAE	PDA + TATB	- Dioxane/mesitylene, −20 °C, −5 °C, r.t., 150 °C, 3 days - $Pd(OAc)_2$ solution in DCM	40
14	Pd(0)/TAT–DHBD	TAT + DHBD	- Dioxane/mesitylene/ACOH, 120 °C, 3 days - $Pd(OAc)_2$ solution in DCM	41
15	Pd(0)/TAT–TFP	TAT + TFP	- Dioxane/mesitylene/ACOH, 120 °C, 3 days - $Pd(OAc)_2$ solution in DCM	41
16	Pd/NCNs	*p*-Phthalaldehyde + melamine	- Benzene, 105 °C, 24 h - Carbonization at 700 °C, 2 h - $Pd(OAc)_2$ solution in MeOH, reflux for 12 h	42
17	Pd@CTF	Melamine + cyanuric chloride	- DMF/Et_3N, 120 °C, 24 h - H_2PdCl_4 solution, $NaBH_4$	43
18	Pd@COF-Ph	Cyanuric chloride + PDA	- Dioxane/K_2CO_3, 90 °C, 3 days - Aqueous solution of $PdCl_2$ in *n*-hexane, $NaBH_4$	45
19	Pd/TPA-TCIF	TFPA + TAPT	- *n*-Butanol/DCB/AcOH, 120 °C, 72 h - $Pd(OAc)_2$ solution in DCM, reflux for 3 h	46
20	Pd/TFPT-Azine-COF	TFPT + hydrazine	- (Bu_4NBr/Im) DES solvent, 90 °C, 12 h - $Pd(OAc)_2$ solution in DCM, reflux for 3 h	47
21	Pd NPs@TTT-COF	TTI-COF + S_8	- TTI-COF + S_8, 155 °C (3 h) → 350 °C (3 h)	48
22	Pd@COF-TM	Trimesoyl chloride, melamine	- DCM/Et_3N, r.t, 24 h - $Pd(OAc)_2$ solution in acetonitrile	50
23	Pd@OC-MA	Melamine + OC	- THF/Na_2CO_3, 40 °C, 24 h - $Pd(OAc)_2$ solution in acetonitrile	51
24	Pd@PCOFs	Melamine + BPDA	- Calcination in 325 °C for 4 h - Dispersed $Pd(OAc)_2$ in water, $NaBH_4$	52
25	Pd@CTF-1	1,4-Dicyanobenzene	- Trimerization of catalyzed by triflic acid at 250 °C - Calcination at 350 °C - $Pd(OAc)_2$ solution in DCM	53
26	PdNPs@Thio-COF	Tp + thioether substituted diamine	- Dioxane/mesitylene/AcOH, 120 °C, 3 days - K_2PtCl_4 in MeOH, $NaBH_4$	54
27	Pd@COF-AO	Tp + BATH	- Dioxane/mesitylene/AcOH, 120 °C, 3 days - $Pd(OAc)_2$ solution in toluene	55
28	Pd@COF-NHC	TAB + NFB	- [BMIm][NTf_2] ionic liquid, r.t., 3 days - $Pd(OAc)_2$ solution in acetonitrile, 75 °C, 3 h	56
29	Pd/COF-SO_3H	Tp + DASA	- *n*-Butanol/DCB/AcOH, 120 °C, 3 h - $Pd(NO_3)_2$ in water, $NaBH_4$	57
30	Pd@COF-QA	L-QA + TFB	- Dioxane/mesitylene/AcOH, 120 °C, 3 days - $Pd(OAc)_2$ solution in DCM, Et_3N 50 °C, 24 h	58

Table 2 (*Contd.*)

Entry	COFs	Precursors[a]	Synthesis procedure	Ref.
31	Pd/H_2P-Bph-COF	H_2TAPP + BPA	- EtOH/mesitylene/AcOH, 120 °C, 3 days - $Pd(OAc)_2$ solution in DCM	60
32	Mn/Pd@Py-2,20-BPyPh	PyTTA + 2,2′-BPyDCA	- Dioxane/mesitylene/AcOH, 120 °C, 3 days - $MnCl_2 \cdot 4H_2O$ solution in MeOH - $Pd(OAc)_2$ solution in DCM	62 63
33	Pd@TpBpy	Tp + Bpy-$PdCl_2$	- DMAC/dioxane/AcOH, 90 °C, 3 days	66
34	Pd@TpTe-1	Tp + TPH	- Dioxane/mesitylene/AcOH, 120 °C, 3 days - $Pd(NO_3)_2$ solution in MeOH	69
35	PdNPs@CON–DAI–TFP Pd@COF–DAI–TFB	DAI + TFP DAI + TFB	- DCB/MeOH/AcOH, 100 °C, 3 days - K_2PdCl_6 solution in ethanol/water	71
36	Pd@COF-BTDH	TFB + DHB	- Dioxane/*n*-butanol/AcOH, 120 °C, 3 days - $Pd(OAc)_2$ solution in DCM	72
37	PdNPs@Phos-COF-1	PDA + TFPP	- Dioxane/mesitylene/AcOH, 120 °C, 3 days - K_2PdCl_4 in MeOH solution	73
38	Pd@COF-SMC2	Tp + PDA	- EtOH, r.t., 30 min - DMF, 160 °C, 4 h - $Pd(OAc)_2$ solution in DCM	75
39	Pd@Phen-COF	Phenanthroline building block + TAPB	- Dioxane/mesitylene/AcOH, 120 °C, 3 days - $Pd(OAc)_2$ solution in acetonitrile, 70 °C, 16 h	76
40	CNT–COF–Pd	TFPPy + PDA + CNT	- Dioxane/AcOH, 120 °C, 3 days - $PdCl_2$ solution in MeOH/water, $NaBH_4$	78
41	Pd@COF-102	TBPM	- Dioxane/mesitylene, 85 °C, 4 days - $Pd(\eta^3\text{-}C_3H_5)$ $(\eta^5\text{-}C_5H_5)$, UV-light irradiation	80
42	COF-300	TAM + TPA	- Dioxane/AcOH, 120 °C, 3 days - $Pd(OAc)_2$ solution in DCM	82
43	Pd(II)@SP-3D-COF-BPY	SBFTA + BPDC	- Phenylmethanol/mesitylene/AcOH, 120 °C, 3 days - $Pd(OAc)_2$ solution in DCM, $NaBH_4$	84
44	Pd@TPM-3D-COF-BPY	TAM + BPDC	- Phenylmethanol/mesitylene/AcOH, 120 °C, 3 days - K_2PdCl_4 solution in methanol, $NaBH_4$	85

[a] TFB: 1,3,5-triformylbenzene; PDA: *p*-phenylenediamine; DCM: dichloromethane; PTSA: *p*-toluenesulfonamide; TRIF: tri-(4-formacylphenoxy)-1,3,5-triazine; TATB: 4,4′,4″-(1,3,5-triazine-2,4,6-triyl)tribenzaldehyde; TAT: 1,3,5-tris(4′-aminophnyl)triazine; DHBD: 2,5-dihydroxybenzene-1,4-dicarboxaldehyde; TFP: 1,3,5-triformylphloroglucinol; TAPT: 2,4,6-tris(4-aminophenyl)triazine; TFPA: tris(4-formylphenyl)amine; TFPT: 2,4,6-tris (5-formyl-2-pyridinoxy)- 1,3,5-triazine; OC: 4,4-oxydibenzoyl chloride; BPDA: 3,3′,4,4′-biphenyltetracarboxylic dianhydride; BATH: 2,5-bis(allyloxy) terephthalohydrazide; TAB: 1,3,5-triaminobenzene; NFP: bi-NHC substituted 1,4-di(4-formylbenzyl)-benzene; DASA: 2,5-diaminobenzene sulfonic acid; H_2TAPP: 5,10,15,20-tetra(*p*-amino-phenyl)porphyrin; BPA: 4,4′-biphenyldialdehyde; PyTTA: 4,4′,4″,4‴-(pyrene-1,3,6,8-tetrayl) tetraaniline; 2,2′-BPyDCA: 2,2′-bipyridine-5,5′-dicarbaldehyde; Bpy-$PdCl_2$: 2,2′-bipyridine-5,5′-diamine palladium chloride; DMAC: *N*,*N*-dimethylacetamide; DAI: 1*H*-indazole-4,7-diamine; TPH: terephthalohydrazide; DHB: 3,3′-dihydroxybenzidine; TFPP: tri-(4-formylphenyl)phosphine; TFPPy: 1,3,6,8-tetrakis(pformylphenyl)pyrene; TBPM: tetra(4-dihydroxyborylphenyl)methane; TAM: tetrakis(4-anilyl)methane; TPA: terephthaldehyde; SBFTA: 9,9′-spirobi[fluorene]-3,3′,6,6′-tetraamine; BPDC: [3,3′-bipyridine]-6,6′-dicarbaldehyde.

Fig. 3 Preparation of Pd doped TiATA@LZU1 core–shell (reproduced from ref. Sun *et al.*, *Adv. Funct. Mater.*, 2018, **28**, 1707110 copyright 2018 WILEY-VCH Verlag GmbH & Co. KGaA, Weinheim).

p-phenylenediamine (Pa-1) under solvothermal conditions (Table 2, entry 6).[29] This COF is used widely for stabilizing Pd catalysts. Banerjee and co-workers immobilized Pd nanoparticles into the TpPa-1 framework (Pd@TpPa-1) (Fig. 6). They found that treatment of the host COF with palladium acetate followed by reduction did not change the crystallinity and basic architecture of the framework. The reduction of the surface area of TpPa-1 from 484 $m^2\ g^{-1}$ to 195 $m^2\ g^{-1}$ for Pd@TpPa-1 confirmed the fine dispersion of nanoparticles in the pores and between the layer spaces of the COF. Also, XPS measurements and comparison to Pd–N interaction in the Pd–phenanthroline complex showed a positive shift of the binding energy by 0.7 eV for the N 1s region, which proves a strong interaction of palladium and the imine-nitrogen atoms. Morphological studies of this catalyst indicate Pd NPs that were well dispersed throughout the material with 7 ± 3 nm average size. The thermocatalytic activity of Pd@TpPa-1 was studied in copper and ligand-free Sonogashira, Heck, and one-pot sequential Heck–Sonogashira coupling reactions and a range of products were obtained in excellent yield (70–95% isolated yield).[30]

Lu and co-workers investigated the activity of previously reported Pd^0/COF-LZU1 and Pd^0/TpPa-1 for photocatalytic H_2 production. Both of them showed higher hydrogen production related to Pd/C but Pd^0/TpPa-1 has much higher activity (10 times) and the hydrogen production rate under visible light

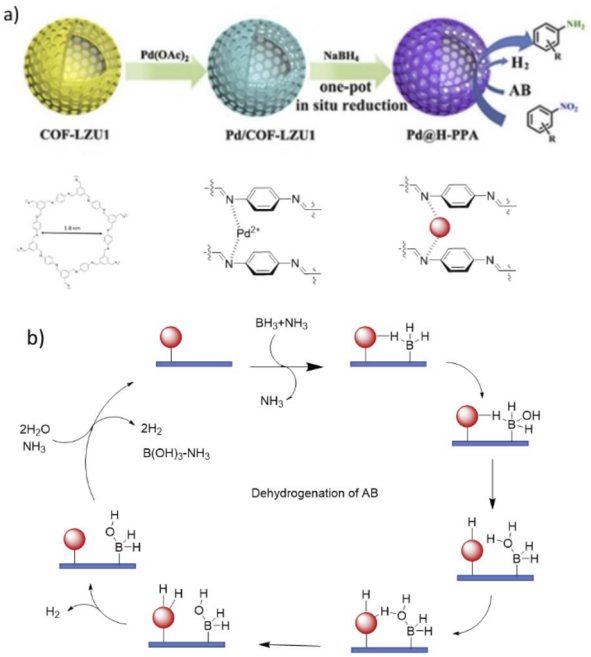

Fig. 4 (a) Synthesis procedure of Pd@H-PPA and its catalytic applications, (b) dehydrogenation mechanism of ammonium borane (AB).

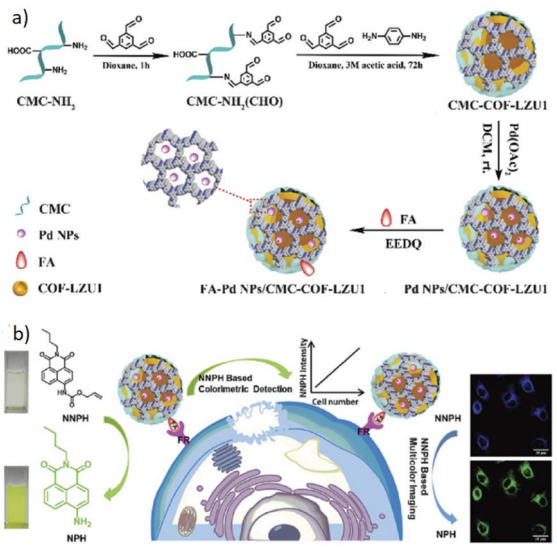

Fig. 5 (a) Synthesis process of FA–Pd NPs/CMC-COF-LZU1 (b) schematic illustration for cancer cell imaging by FA–Pd NPs/CMC-COF-LZU1 (reproduced from ref. Sun *et al.*, *Nanoscale*, 2020, **12**, 825–831 with permission from the Royal Society of Chemistry).

irradiation using triethanolamine (TEOA) as a sacrificial reagent and Eosin Y (EY) as the sensitizer was. The authors pose that this high photocatalytic efficiency is related to the carrier role of the conjugated COF in facilitating the transfer of photogenerated electrons.[31]

In 2019 a yolk–shell nanostructures based on TpPa-1 as a shell was designed and reported by Yu *et al.* Pd NPs were first coated with zeolite imidazolate frameworks-8 (ZIF-8) to form

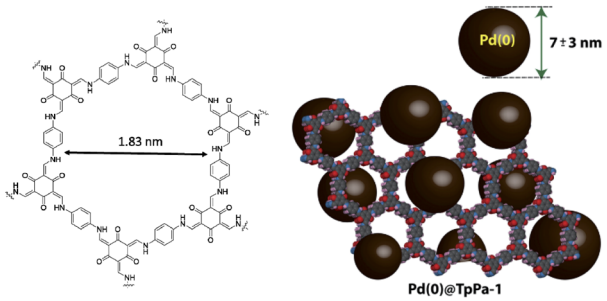

Fig. 6 Structure of TpPa-COF and Pd@TpPa.

Pd@ZIF-8 core–shell structures. On this material an amorphous polyimine network was created by condensation of *p*-phenylenediamine and 1,3,5-triformylphloroglucinol. ZIF-8 was removed by acidic etching in a dioxane/aqueous acetic acid mixture, during which the amorphous polyimine shell was transferred in a crystalline COF and the yolk–shell Pd@H-TpPa was formed (Fig. 7) (Table 2, entry 7). The main advantage of using a COF as shell is the allowance for efficient mass transport through the thin shells. The surface area of the composite material was only 42 m^2 g^{-1}, much lower than TpPa COF.[32]

The catalytic activity of Pd@H-TpPa was investigated in the reduction of nitrobenzene with $NaBH_4$ at room temperature. This reaction took place with high activity and selectivity in only 8 minutes. Interestingly, the authors found that the catalytic activity of Pd@H-TpPa depended on the shell thickness with the reaction rate decreasing by increasing shell thickness. The morphological studies of the catalyst after recycling proved that the TpPa-1 COF shell protects Pd nanoparticles from aggregation during the reaction.

Also, encapsulation of Pd NPs by yolk–shell structure in the TpPa COF to make a shell to confined Pd NPs was done by Zhang and co-workers (Fig. 8). TpPa-1 was grown on the surface of functionalized (Pd/C)@SiO_2, and followed by etching a SiO_2 layer in HF (Table 2, entry 8). The important advantage of this shell is its protection against the leaching of palladium, strong interaction with Pd nanoparticles because of the nitrogen enrichment, and the uniform pore sizes that make unique molecular-size selectivity. The porosity analysis of the (Pd/C)@TpPa showed a surface area of 166 m^2 g^{-1} and 1.29 nm pore sizes.

The catalytic activity of the (Pd/C)@TpPa was explored in the Suzuki–Miyaura coupling reaction at 80 °C under N_2

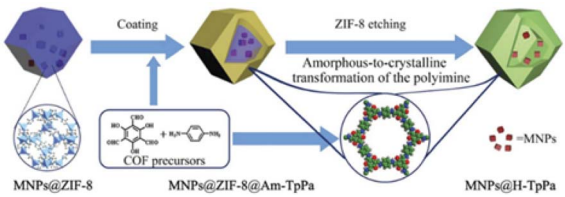

Fig. 7 Synthesis procedure of Pd@H-TpPa (reproduced from ref. Cui *et al.*, *Small*, 2019, **15**, 1–8 copyright 2018 WILEY-VCH Verlag GmbH & Co. KGaA, Weinheim).

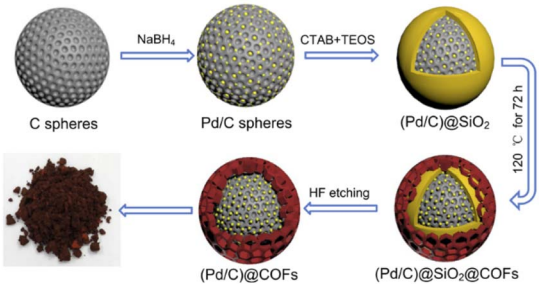

Fig. 8 Schematic synthesis procedure of (Pd/C)@TpPa (reproduced from ref. Li *et al.*, *J. Colloid Interface Sci.*, 2021, **591**, 273–280 copyright 2021 Elsevier Inc. All rights reserved).

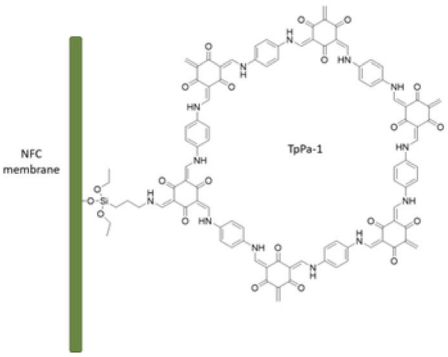

Fig. 9 Structure of Pd@COF/NFC membrane.

atmosphere which showed a high yield and excellent recyclability (Table 1, entry 2). Moreover, because of the small pore size of the COF shell, it strongly depends on the molecular size of the reactant and product. The conversion for the reactant with a phenyl functional group decreased to 14%, and coupling of 1,3,5-tris(4-iodophenyl)benzene and phenyl boronic acid dropped dramatically to 0.4%.[33]

Chen and co-workers used a Pd@TpPa-1 COF for phenol hydrogenation. The influence of different ratios of water and acetic acid on the morphology, crystalline structure and stacking degree of TpPa-1 was studied. Generally, the surface area and strength of π–π stacking are two important factors of the increase in the Pd loading. A lower water ratio caused an improved π–π stacking and made tighter molecular layers. This structure has more binding sites for stabilizing palladium which causes higher loading of palladium (Pd@TpPa-1-0 with 0% water, 2.21% Pd loading). Even though a higher ratio of water caused a higher surface area, because of weaker π–π stacking, the weak interaction of the host COF with metal decreased the loading percentage of palladium (Pd@TpPa-1-100 with 100% water, 0.65% Pd loading). The higher surface area for Pd@TpPa-1-100 is the reason for smaller palladium nanoparticle sizes (2 nm) compared to Pd@TpPa-1-0 with 4.7 nm.[34]

The catalytic activity of Pd@TpPa-1 was evaluated by the hydrogenation of phenol to cyclohexanone under 0.1 MPa H_2 at 90 °C. For Pd@TpPa-1-100, 50% conversion with 98% selectivity was reported, and the catalyst was still stable after five runs. Interestingly, during the catalytically reduction of phenols, Pd^{2+} was reduced to Pd NPs which were trapped in the COF structure.

Zhang *et al.* fabricated a palladium-containing membrane based on loading of palladium in the TpPa-1 COF on the surface of functionalized nanofibrillated cellulose (NFC) (Table 2, entry 9). TpPa-1 was grown on the surface of amino-propyltriethoxysilane functionalized NFC by a bottom-up synthesis strategy (Pd@COF/NFC) (Fig. 9). The XRD pattern of the COF/NFC membrane was matched with TpPa-1, and the surface area (357 m^2 g^{-1}) and pore sizes (2–20 nm) proved the crystallinity and regularity of the structure. The impregnation of the membrane with palladium was done by coordination with palladium acetate followed by reduction with $NaBH_4$. The dechlorination process of *o*-dichlorobenzene was studied with the Pd@COF/NFC membrane, which showed a very high activity and recyclability for the prepared membrane.[35]

Chen and co-workers used TpPa-1 COF to stabilize Pd NPs. TpPa-1 was prepared by calcination at different temperatures, in the presence of different ratios of *p*-toluenesulfonamide (PTSA) (Table 2, entry 10). Palladium impregnation was done by stirring the COF with $Pd(OAc)_2$ in methanol (Fig. 10). A uniform spherical shape COF was prepared at 280 °C with the highest surface area (52.2 m^2 g^{-1}) in the BET analysis, although the surface area is lower for TpPa-1 in this method compared to the conventional solvothermal methods (195 m^2 g^{-1}). Morphological analysis of the Pd@COF-280 showed Pd NPs with a 6.7 nm average size. This palladium/COF hybrid was used for the hydrogenation of phenol, so Pd^{2+} is reduced to Pd^0 during the reaction process. They have found that the morphology of the TpPa-1 COF strongly depends on the calcination temperature. The catalytic activity of Pd@COF-280, as the best catalyst investigated at a hydrogen pressure of 0.1 MPa and a reaction temperature of 80 °C, showed excellent conversion and selectivity for the hydrogenation of phenol to cyclohexanone.[36]

2.3 Triazine-based COFs

Dong *et al.* anchored palladium nanoparticles in a chiral covalent organic frameworks as a highly active heterogeneous catalyst for asymmetric Henry and Heck reactions with high stereoselectivity and yield (Table 2, entry 11).[37] The CCOF-MPC was prepared by heating the mixture of *S*-(+)-2-methylpiperazine and cyanuric chloride at 90 °C in the presence of K_2CO_3 and the

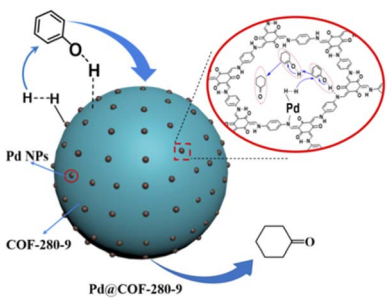

Fig. 10 Schematic structure of Pd@COF-280 in the reaction process (reproduced from ref. Jiang *et al.*, *Ind. Eng. Chem. Res.*, 2021, **60**, 13523–13533 copyright 2021, American Chemical Society).

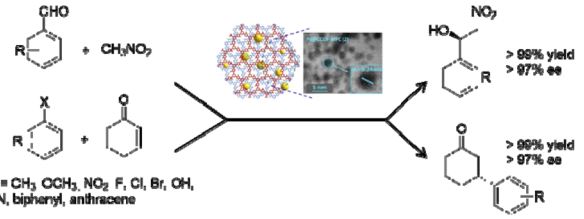

Fig. 11 Catalytic application of Pd@CCOF-MPC.

final Pd@CCOF-MPC catalyst was prepared by reducing Pd^{2+} impregnated in the COF by simple physical stirring of $Pd(NO_3)_2$ and the host COF in MeOH.

The BET analysis indicated 686 $m^2\ g^{-1}$ surface area for Pd@CCOF-MPC and pore size of the COF of 1.5 nm. The size of the palladium nanoparticles was 2–5 nm, which is much larger than the pore size. This proves that the nanoparticles are dispersed between layers of the COFs and are stabilized with nitrogen atoms.

The catalytic activity of Pd@CCOF-MPC was evaluated in the synthesis of chiral β-nitro alcohols by a Henry reaction in ethanol at room temperature, with excellent yield and enantioselectivity (80–99%) without any additive (Fig. 11). In recycling experiments, the palladium did not leach and after five runs still kept its activity (>90% yield). Moreover, the catalyst was used as a heterogeneous asymmetric catalyst for reductive Heck reaction, in aqueous ethanol at 80 °C, for the first time. A large scope of products with very high yield and selectivity (80–99%) was synthesized using this catalyst. Interestingly, polycyclic substrates do not react, demonstrating that the reaction takes place within the pore of material.

Zhang *et al.* used an electron-rich triazine-based COF for immobilizing palladium, gold, and platinum. The COF-SDU1 is synthesized by the solvothermal condensation method of tri-(4-formacylphenoxy)-1,3,5-triazine (TRIF) and *p*-phenylenediamine. Palladium was dispersed in the framework by stirring $Pd(OAc)_2$ and the COF in dichloromethane (Table 2, entry 12). Pd^{2+} strongly coordinates with the imine and triazine groups of COF-SDU1. The pristine COF-SDU1 possessed a BET surface area of 1125 $m^2\ g^{-1}$, which after coordination with Pd^{2+} only dropped to 1052 $m^2\ g^{-1}$.[38]

Pd(II)/COF-SDU1 showed high activity and selectivity for a one-pot reaction of silane oxidation and cross-coupling with aryl iodide (Fig. 12). Palladium does not leach from the catalyst, and the recycling test proved it could be use in at least four runs without losing any activity.

Vaidhyanathan *et al.* used the same COF to stabilize Pd nanoparticles to make an efficient catalyst for the Heck coupling reaction. Pd-trzn-COF with a 18–20% palladium content was prepared by loading Pd^{2+} in an ethanolic solution. According to the authors, because of the nitrogen-rich structure of the COF, the reduction of Pd^{2+} to Pd^0 could be done *in situ* without any reducing agents.[39]

Another type of triazine base COF was designed and reported by Siva *et al.* as a new host to immobilize palladium (Pd/TATAE). The TATAE COF was synthesized by condensing 4,4′,4″-(1,3,5-triazine-2,4,6-triyl)tribenzaldehyde and 1,4-diaminobenzene.

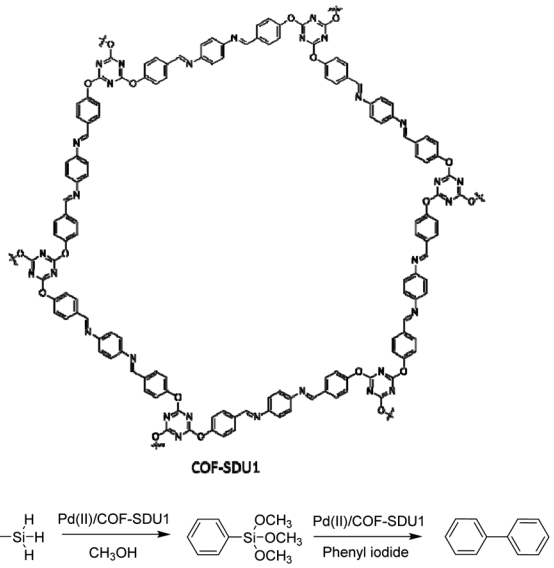

Fig. 12 Structure of COF-SDU1 and application of Pd(II)/COF-SDU1 in one-pot silane oxidation/cross-coupling reaction.

The reagents were slowly added at −20 °C in THF and kept at −5 °C for 2 hours. Then, the temperature was increased to 150 °C and it was kept at this temperature for 72 h. Palladium impregnation of the synthesized COF (Pd/TATAE) was performed by physical stirring of the COF and Pd(OAc) in DCM at room temperature (Table 2, entry 13).[40] The negative shift of Pd and the positive shift of nitrogen in XPS analysis is a prove for the strong coordination of Pd with the imine-nitrogens of the COF.

The catalytic activity of Pd/TATAE was investigated in the Suzuki–Miyaura coupling reaction using green conditions (Table 1, entry 3). A wide variety of substrates could be reacted in water as the solvent at room temperature with excellent yields.

Murugavel and co-workers synthesized two new triazine-based imine and β-ketoenamine linked COFs, TAT–DHBD and TAT–TFP (Fig. 14) by condensation reaction of 1,3,5-tris(4′-aminophnyl)triazine (TAT) with 2,5-dihydroxybenzene-1,4-dicarboxaldehyde (DHBD) or 1,3,5-triformylphloroglucinol (TFP) under solvothermal condition (Table 2, entry 14, 15).[41]

The BET surface areas for TAT–TFP and TAT–DHBD were 646 $m^2\ g^{-1}$ and 1750 $m^2\ g^{-1}$, respectively. The pore sizes were 11.7 Å for TAT–TFP whereas TAT–DHBD had two pore diameters: 26.1 and 37.9 Å with the second one related to the swelling effects at 77 K, which is seen from the hysteresis in the low pressure region.

Palladium loading on the COFs was performed by physical stirring and reduction by $NaBH_4$. The XRD pattern of the prepared Pd(0)/TAT–DHBD and Pd(0)/TAT–TFP indicates they kept their crystallinity. The pore size of the COFs decreased after reduction of Pd^{2+} to Pd^0 nanoparticles. Morphological studies of the Pd/COFs show Pd NPs with <5 nm particles uniformly dispersed in the lattice of the COFs.

The catalytic activity was evaluated by Suzuki–Miyaura coupling reaction in THF at 100 °C with good to excellent yield

and high selectivity for cross-coupling reactions (Table 1, entry 4–7).

Dong and co-workers constructed Pd dispersed nitrogen-doped carbon nanosheets (NCN) through carbonization of 2D-triazine-based COFs prepared by condensation of *p*-phthalaldehyde and melamine under solvothermal conditions (Fig. 15) (Table 2, entry 16).[42]

The high nitrogen content (32.71%) of the NCN support provides electrons for coordination with Pd NPs and prevents aggregation or sintering. The prepared catalyst is used for hydrodechlorination (HDC) of chlorophenols, highly toxic environmental pollutants. Pd/NCN showed complete conversion and selectivity for HDC of different chlorophenols in an aqueous solution and 1 bar H_2 pressure at room temperature. Interestingly, with increasing the temperature to 80 °C, high conversion and selectivity to cyclohexanone was observed for chlorophenols.

Wang and co-workers designed and used a Pd anchored triazine-based covalent organic framework to reduce nitroarenes by catalytic hydrogenation with formic acid. The Pd@CTF was synthesized by the solvothermal method with cyanuric chloride and a melamine mixture in a steel autoclave, impregnation with Pd^{2+}, and reduction (Fig. 16) (Table 2, entry 17). The morphological studies of the final catalyst proved uniformly dispersed Pd nanoparticles in the host framework with an average size of 4.25 nm.[43]

The catalytic activity of the catalyst was investigated in the reduction of a wide range of nitroarenes, using an aqueous solvent, at room temperature, which resulted in excellent yield and selectivity (>99%).

Moreover, in 2018 Sadhasivam *et al.* used imine-linked triazine-based TATAE COF (Fig. 13) to stabilize Pd nanoparticles with the interaction of Pd NPs and imine groups. They used Pd/TATAE as a catalyst in Mizoroki–Heck coupling reaction in DMF/water at 70 °C.[44]

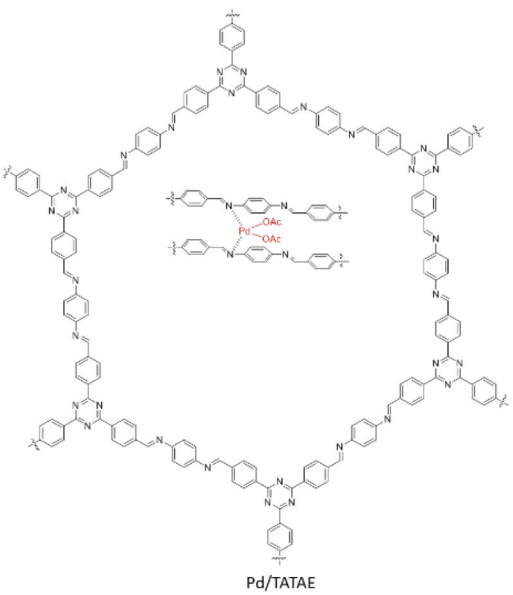

Fig. 13 Structure of Pd/TATAE.

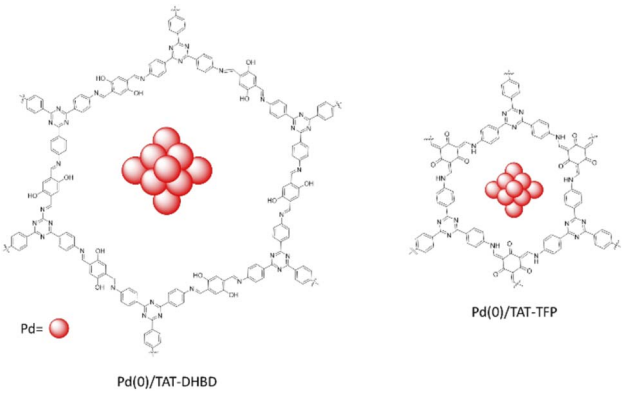

Fig. 14 Schematic structure of Pd(0)/TAT–DHBD and Pd(0)/TAT–TFP.

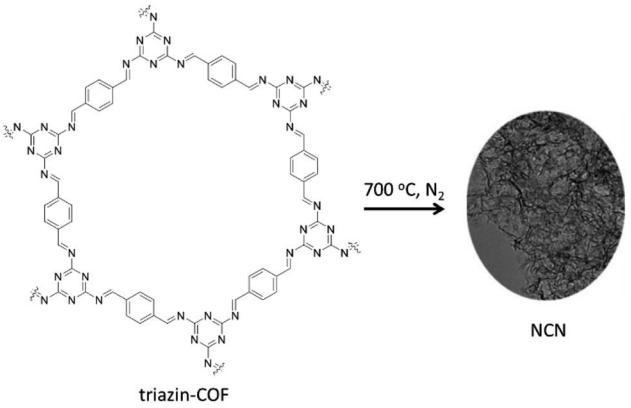

Fig. 15 Carbonization of triazine-COF to NCN.

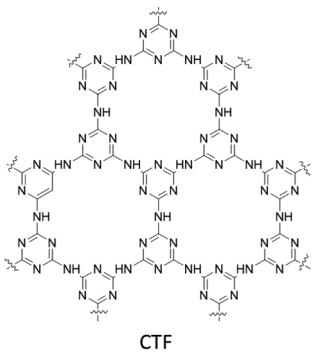

Fig. 16 Structure of CTF.

Dong *et al.* fabricated two triazine-based COFs with different pore sizes to immobilize the Pd nanoparticles. The COFs were prepared by a condensation reaction of cyanuric chloride and *p*-phenylenediamine (COF-Ph) or 4,4′-diaminobiphenyl (COF-BPh). Pd clusters were then anchored in the COFs pores by coordination and reduction (Table 2, entry 18). The average sizes of the Pd clusters are 0.79 and 0.81 nm for the Pd@COF-Ph and Pd@COF-BPh COFs, respectively, which were immobilized in the pore of the COFs with an average size of 2.3 nm and 3.8 nm. The main reason for the small and narrow size

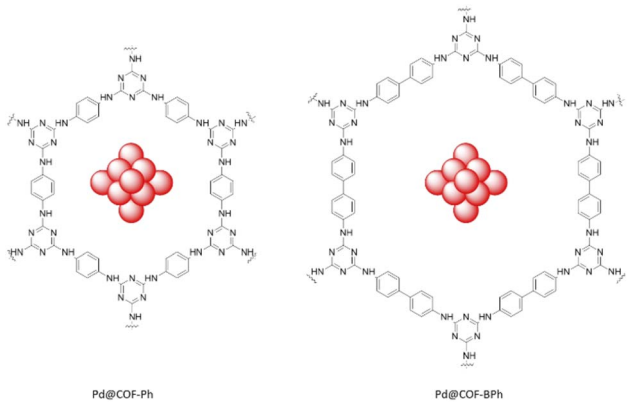

Fig. 17 Structure of Pd@COF-Ph and Pd@COF-BPh catalysts.

distribution of the palladium nanoparticles are the confinement of palladium in the pores of the frameworks (Fig. 17).[45]

The catalytic activity of the prepared Pd/COFs was studied in the nitroarene reduction reaction with $NaBH_4$ as the hydrogen source in an aqueous solvent at 25 °C. Both of them are catalytically active, but Pd@COF-BPh has a higher activity because of its larger pore size. A wide variety of nitroarenes could be reduced by this catalyst with excellent yields (77 to 99%).

Ahn *et al.* fabricated palladium immobilized imine-linked triazine-based COF (Pd/TPA-TCIF) and used it for the cyanation of haloarenes. TPA-TCIF COF was prepared by condensation 2,4,6-tris(4-aminophenyl)triazine and tris(4-formylphenyl) amine under solvothermal conditions (Fig. 18). The final catalyst was prepared by impregnating Pd^{2+} by stirring the COF and $Pd(OAc)_2$ in dichloromethane (Table 2, entry 19). The prepared TPA-TCIF and Pd/TPA-TCIF possessed very high surface areas of 2938 and 2647 $m^2\ g^{-1}$, respectively, and 1.5 nm pore sizes.

Pd/TPA-TCIF was explored in the catalytic cyanation of haloarenes with $K_4[Fe(CN)_6]$ as a source of nitrile groups with high yield (60–100%). The Pd/TPA-TCIF was stable and recyclable under the reaction conditions (110 °C for 20 h).[46]

Zhang and co-workers prepared an azine linked Pd/TFPT-Azine-COF by the condensation reaction of 2,4,6-tris (5-formyl-2-pyridinoxy)-1,3,5-triazine (TFPT) and hydrazine in a deep eutectic solvent (DES) composed of tetrabutylammonium bromide and imidazole (Bu_4NBr/Im). Then, $Pd(OAc)_2$ was impregnated in a dichloromethane solution (Table 2, entry 20). The surface areas measurement showed 328 and 64 $m^2\ g^{-1}$ for the TFPT-Azine-COF and the Pd/TFPT-Azine-COF, respectively, and a pore size of 2–3 nm, indicating the presence of mesopores (Fig. 19). The catalytic Hirao cross-coupling reaction between aryl halides and dialkyl phosphites could be catalyzed by Pd/TFPT-Azine-COF with good yield (50 to 95%) in refluxed cyclopentyl methyl ether (Fig. 19).[47]

A benzothiazole-linked COF (TTT-COF) was prepared by Cai and co-workers as host material for Pd nanoparticles to use in photocatalytic C–C cross-coupling reactions. The COF was prepared by a previously reported[48] post-synthetic sulfuration strategy of the corresponding imine-linked COF (TTI-COF), followed by palladium coordination and reduction to Pd^0 with $NaBH_4$ resulting in Pd NPs@TTT-COF with a surface area of 1025 $m^2\ g^{-1}$ (Fig. 20) (Table 2, entry 21).

The palladium nanoparticles of the benzothiazole had a size of 2.01 nm, much smaller than the imine linked COF, whose nanoparticles had a size of 6.3 nm. This is related to the anchoring of palladium to the S atoms confining them in the pores of the COFs and reducing their size.

The prepared Pd NPs@TTT-COF was used as a photocatalyst in the Suzuki–Miyaura cross-coupling reaction under visible

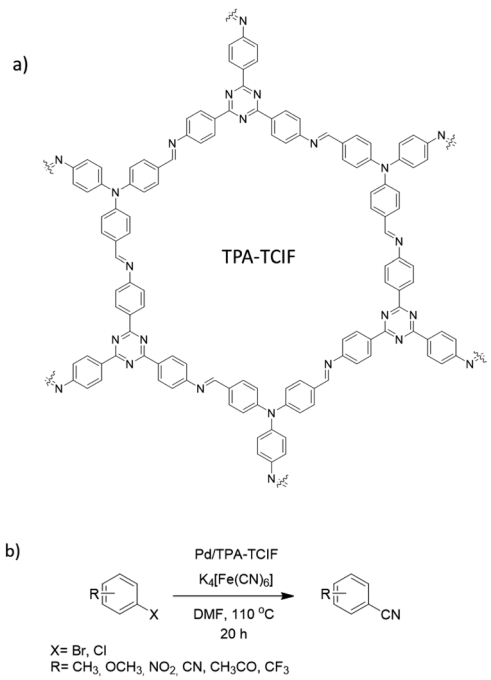

Fig. 18 (a) Structure of TPA-TCIF, (b) catalytic cyanation of haloarenes.

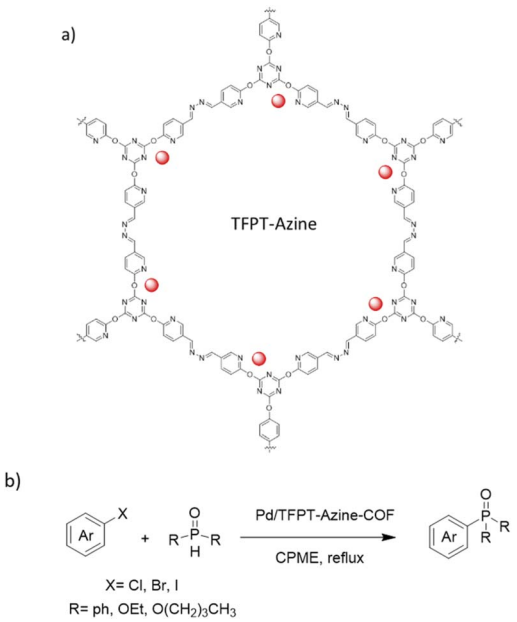

Fig. 19 (a) Structure of TPA-TCIF, (b) Hirao cross-coupling reaction.

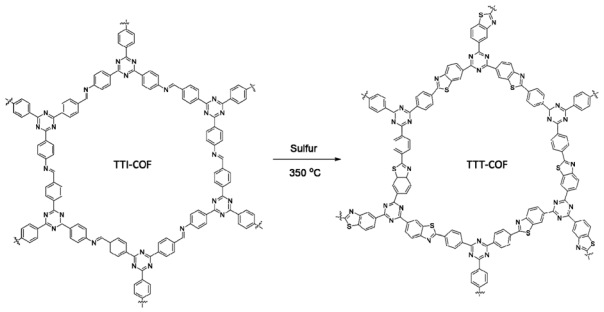

Fig. 20 Schematic synthesis procedure of TTT-COF from TTI-COF.

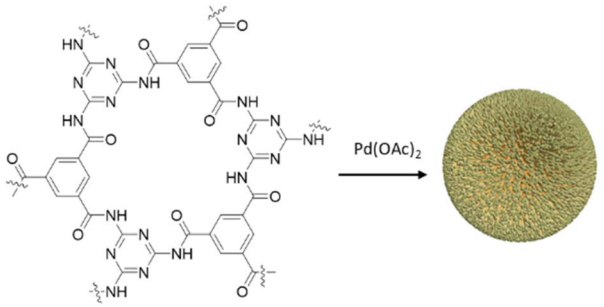

Fig. 21 Structure of Pd@COF-TM.

light with very high yields. According to the suggested mechanism, electrons were excited by light from the valence bond (VB) to the conducting bond (CB) of the COF and transferred to the Pd nanoparticles to make electron-rich palladium. Palladium under this condition facilitates the cleavage of a carbon–halogen bond to generate the phenyl radical and make an organometallic complex. Another phenyl radical was prepared by C–B bond cleavage by photogenerated holes. These radicals were then coupled to the biphenyl product by reductive elimination. Pd NPs@TTT-COF also showed good activity for Stille, Heck and Sonogashira coupling reactions.[49]

Yang *et al.* synthesized palladium containing amide-linked Pd@COF-TM by condensation of trimesoyl chloride (TMC) and melamine (MA) followed by coordination of $Pd(OAc)_2$ (Fig. 21) (Table 2, entry 22). The XPS analysis showed increase of binding energy for N atoms, and decrease for Pd^{2+} atoms that proves the coordination of palladium with nitrogen atoms. The prepared catalyst possessed excellent activity for the Suzuki–Miyaura coupling reaction in water at room temperature, especially for aryl chlorides as a challenging reactant (Table 1, entry 8). Aryl chlorides with different substitutions were explored and a higher reactivity for electron donating groups was found. Electron withdrawing groups and *ortho*-substituted aryl halides and phenyl boronic acids possessed decreased reactivity. The catalyst could be recycled for nine times with a slight decrease of catalytic activity from 99% conversion to about 80% in the ninth run.[50]

Yang *et al.* prepared Pd@OC-MA through immobilization of $Pd(OAc)_2$ in the OC-MA amide-linked COF which is synthesized by condensation of melamine and 4,4-oxydibenzoyl chloride (Table 2, entry 23). The prepared catalyst worked as an efficient

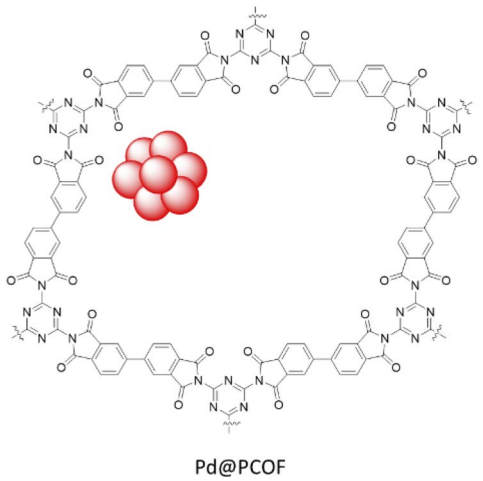

Fig. 22 Structure of Pd@PCOFs.

catalyst for the Suzuki–Miyaura coupling reaction in water at room temperature for a large scope of aryl bromides and chlorides with different substitutions (Table 1, entry 9).[51]

Wang *et al.* synthesized a polyimide linked COF by condensation of melamine and 3,3′,4,4′-biphenyltetracarboxylic dianhydride under calcination conditions at 325 °C followed by palladium coordination and reduction giving rise to Pd@PCOF (Fig. 22) (Table 2, entry 24). The morphological studies showed spherical nanoparticles with a 3–5 nm range. The catalytic activity of the catalyst was investigated in the Suzuki–Miyaura coupling reaction of aryl iodides in water at 80 °C which resulted in yield of >90%. Moreover, the reduction of nitroarenes by $NaBH_4$ was investigated in water at room temperature and showed excellent yields (85 to 99%).[52]

Dong and co-workers used covalent triazine frameworks (CTFs) as stable, nitrogen-rich carrier materials for Pd NPs. The CTF-1(AB) was prepared by trimerization of 1,4-dicyanobenzene catalysed by trifluoromethanesulfonic acid at 250 °C followed by calcination at 350 °C to prepare CTF-1(AA). Pd@CTF-1 was prepared by coordination of CTF-1(AB) with palladium acetate, calcination at 350 °C, and reduction with H_2 at 250 °C (Table 2, entry 25). The surface area was 641 $m^2\ g^{-1}$ for CTF-1, and interestingly did not decreased by loading Pd NPs. TEM image of the catalyst showed ultrafine, highly dispersed Pd NPs with an average size of 2.29 nm.

The catalytic activity of Pd@CTF-1 was investigated in a one-pot *N*-alkylation reaction under 1 atm H_2 at 60 °C. A wide range of substrates could be transformed in high conversions (72 to 100%) and selectivity in catalytic condensation–hydrogenation and hydrogenation–condensation–hydrogenation reactions (Fig. 23).[53]

2.4 Functionalized covalent organic framework

Zhang and co-workers designed a thioether-containing COF by condensation of 1,3,5-triformylphloroglucinol (Tp) and thioether substituted diamine under solvothermal conditions, followed by loading palladium with a K_2PdCl_4 solution and reduction (Table 2, entry 26). The authors increased the control on the size of the nanoparticles by using a strong interaction of

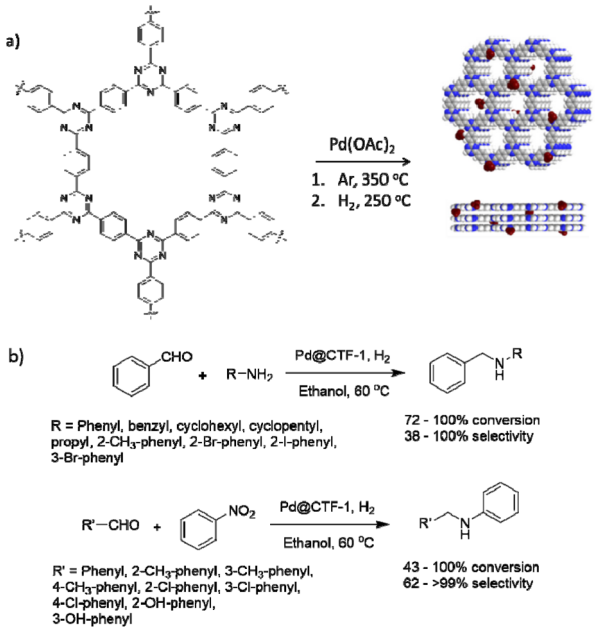

Fig. 23 (a) Structure CTF-1 and Pd@CTF-1, (b) catalytic condensation–hydrogenation and hydrogenation–condensation–hydrogenation reactions.

metal–sulfur binding inside the framework's pores (Fig. 24). The theoretical pore size of Thio-COF was determined to be 2.4 nm, and surface area is 50 $m^2\ g^{-1}$.

The higher interaction of the metal ions with the thioether functional groups confined inside the pores of the Thio-COF during the reduction procedure, caused an increased control on the size of the nanoparticles. The prepared Pd/COF hybrid PdNPs@Thio-COF possesses ultrafine and highly dispersed Pd NPs with a narrow size distribution (1.7 ± 0.2 nm) and 26.30 wt% Pd content.[54]

The catalytic activity of PdNPs@Thio-COF was studied in the Suzuki–Miyaura coupling reaction and showed a high activity in an aqueous solvent and at 50 °C (Table 1, entry 10).

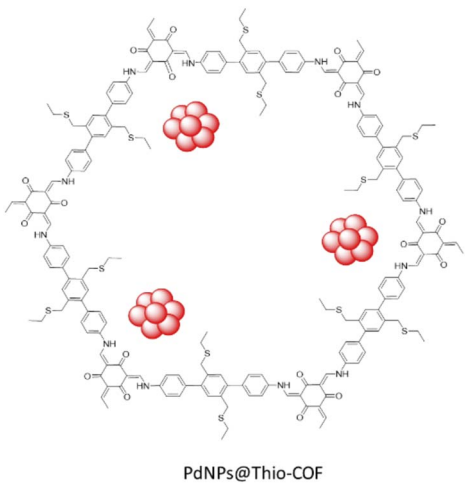

Fig. 24 Schematic structure of PdNPs@Thio-COF.

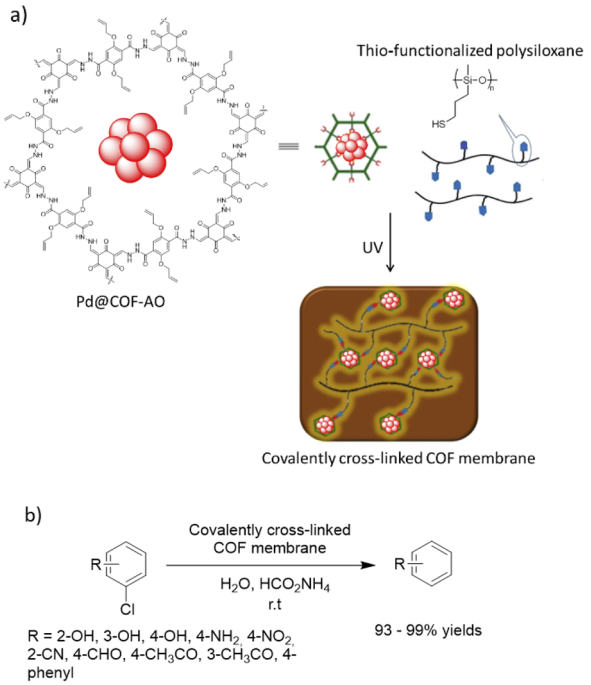

Fig. 25 (a) Synthesis process of covalently cross-linked Pd@COF-AO membrane, (b) dehalogenation of chlorobenzenes (CBs).

Dong and co-workers designed a COF copolymer membrane containing vinyl groups to stabilize palladium nanoparticles (Pd@COF-AO). The host vinyl functionalized COF-AO was prepared under solvothermal conditions by hydrazone bond formation between triformylphloroglucinol (Tp) and 2,5-bis(allyloxy)terephthalohydrazide. Then, Pd(II) was loaded and reduced to Pd nanoparticles by $NaBH_4$ with <5 nm particle sizes (Pd@COF-AO) (Table 2, entry 27). Finally, the membrane was prepared by a thio-ene click reaction of Pd@COF-AO on the thio-functionalized polysiloxane under irradiation of UV light (Fig. 25).[55]

The prepared Pd@COF-AO and membrane was used in the dehalogenation of chlorobenzenes (CBs) in batch and continuous flow. The prepared robust, flexible, water permeable, and processable COF-based membrane showed a very high catalytic activity and yield (93 to 99%) for this important reaction under very mild conditions.

Wang and co-workers used a N-heterocyclic carbene functionalized covalent organic framework (COF-NHC) to stabilize palladium (Fig. 26). The host COF was prepared by the ionothermal condensation of 1,3,5-triaminobenzene (TAB) and the bi-NHC substituted 1,4-di(4-formylbenzyl)-benzene (NFB) in the presence of the ionic liquid 1-butyl-3-methylimidazolium bis((trifluoromethyl)sulfonyl)imide ([BMIm][NTf_2]) (Table 2, entry 28). The prepared Pd@COF-NHC has a 2.7 nm pore size, and XPS studies proved the existence of the Pd^{2+} cation complex in the structure.[56]

The catalytic activity of the Pd@COF-NHC was evaluated in the Suzuki–Miyaura coupling (Table 1, entry 11). The C–C coupling reaction occurred under very mild conditions with

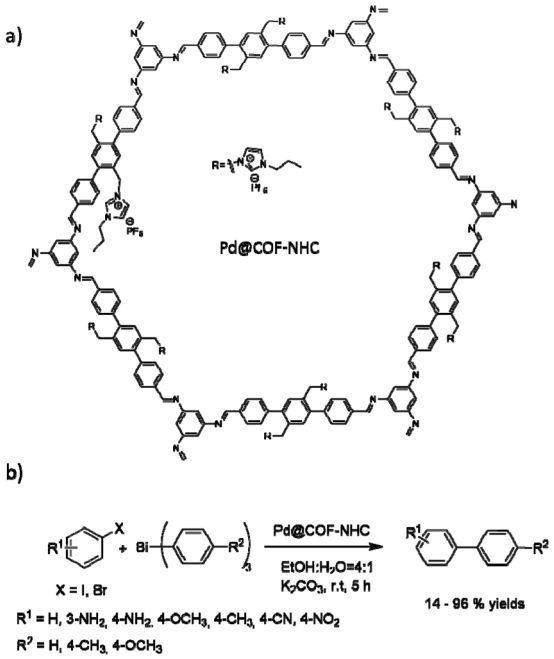

Fig. 26 (a) Structure of Pd@COF-NHC (b) Suzuki–Miyaura cross-coupling reaction.

water as solvent, and at room temperature, with excellent yield (90 to 99%) using Pd@COF-NHC. Moreover, the material could be recycled eight times without significantly losing catalytic activity or change in the crystalline structure of the COF and the Pd^{2+} oxidation state.[56]

Pd@COF-NHC also showed very high activity in cross-coupling triarylbismuths and aryl halides in ethanol/water at room temperature, which usually need dry organic solvents (Fig. 26).

Luo and co-workers designed a SO_3H-anchored COF as a new functionalized host for stabilized palladium NPs. Pd/COF-SO_3H was prepared by condensing 2,4,6-triformylphloroglucinol and 2,5-diaminobenzenesulfonic acid under solvothermal conditions, followed by coordination of a low percentage of Pd (0.38–1.66 wt%) by $Pd(NO_3)_2$ solution and reduction to Pd NPs (Table 2, entry 29). The size of the Pd NPs depended on the palladium loading. With a lower percentage (0.38 wt%) loading the particles average size amounted to 2.63 nm, but with increased loading to 1.66 wt% the particle size increased to 3.24 nm (Fig. 27).[57]

The catalytic activity was studied in the reduction of alkynes to alkenes with very high yield and selectivity using H_2 gas at room temperature. The catalyst was recycled five times and remained stable, active and selective.

Quaternary ammonium groups have been used as a Pd binding group and phase transfer catalyst in a COF synthesized by Don *et al.* The quaternary ammonium salt-decorated dihydrazide linker (L-QA) was prepared in three steps from 2,5-di-(4-methoxycarbonylphenyl) toluene and *N*,*N*-dimethyldodecylamine. COF-QA was prepared by condensation of L-QA and 1,3,5-triformylbenzene under solvothermal conditions in 1,4-

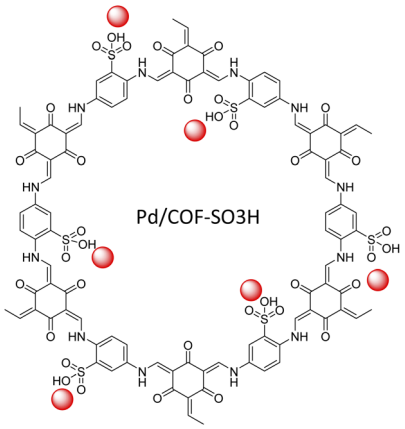

Fig. 27 Schematic structure of Pd/COF-SO_3H.

dioxane/mesitylene at 120 °C. The palladium decoration was performed with palladium acetate solution in dichloromethane followed by *in situ* reduction to Pd NPs by using triethylamine and stirring at 50 °C for 24 h (Table 2, entry 30). Pd nanoparticles dispersed uniformly with a 2.4 nm average size in the Pd@COF-QA framework (Fig. 28). The surface area of COF-QA decreased from 59 to 26 $m^2\ g^{-1}$ by palladium loading.[58]

The catalytic activity of Pd@COF-QA was investigated *via* the Suzuki coupling reaction in water at 50 °C (Table 1, entry 12). Excellent catalytic activity was observed for various substituted aryl halides. Interestingly, it also worked for aryl chlorides as a challenging reactant for the Suzuki–Miyaura coupling reaction. Moreover, the potential of this material on a larger scale application was tested. The prepared COF was combined with chitosan to form a Pd@COF-QA@chitosan aerogel and was applied in a continuous flow reactor. Biphenyl could thus be synthesized on gram scale with 88% yield by coupling of chlorobenzene and phenylboronic acid. The catalyst could be used three times for 8 hours in a continuous flow reactor without a drop in yield, indicating the good stability.

Xu and co-workers prepared a new palladium/COF hybrid by encapsulation of palladium diphosphine complexes into an imine-linked COF through a one-pot self-assembly method.[59]

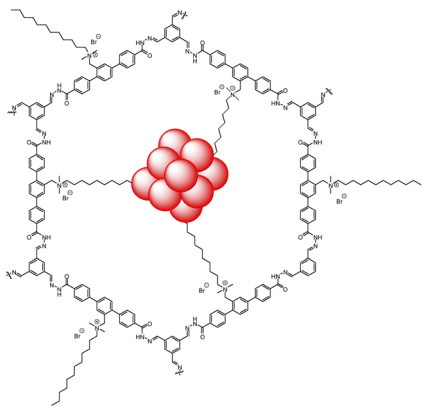

Fig. 28 Structure of Pd@COF-QA.

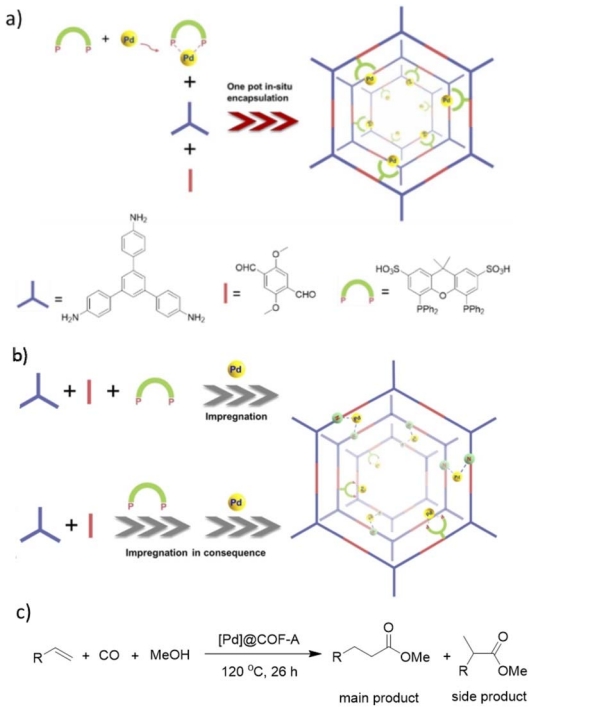

Fig. 29 (a) Schematic of one pot synthesis method of [Pd]@COF-A, (b) impregnation strategies for synthesis [Pd]@COF-B and [Pd]@COF-S, (c) catalytic methoxy carbonylation of terminal alkenes (reproduced from ref. Yang *et al.*, *ChemCatChem*, 2022, **14**, e202101594 copyright 2021 Wiley-VCH GmbH).

The [Pd]@COF was prepared by three strategies. At first a one-pot *in situ* method was used for synthesis of a TPB-DMTP-COF by condensation of the linkers under solvothermal conditions in the presence of $Pd(cod)Cl_2$ and the xantphos-SO_3H ligand ([Pd]@COF-A) (Fig. 29). In the second method the COF was prepared in the presence of xantphos-SO_3H, followed by impregnation of the palladium ([Pd]@COF-B), and in the third method the COF was prepared, followed by impregnation of both the xantphos-SO_3H ligand and palladium ([Pd]@COF-S), separately. The surface area, pore size, and pore volume was higher for the [Pd]@COF-A, prepared by the *in situ* strategy. Also, morphological studies proved uniformly dispersed Pd NPs with an average size of 2.5 nm in the [Pd]@COF-A. The particle sizes of Pd increased to 20 nm by using the impregnation strategies for [Pd]@COF-B and [Pd]@COF-S.

The catalytic activity was investigated in methoxy carbonylation of terminal alkenes under CO (4 MPa) at 120 °C. The *in situ* prepared Pd/COF showed higher activity (100% conversion for styrene) and selectivity (main product: side product = 84 : 16 for styrene).

2.5 Others

Jiang *et al.* used nitrogen-rich porphyrin-based H_2P-Bph-COF to prepare a heterogeneous catalyst for cross-coupling reactions under mild conditions. The COF was prepared by condensing 5,10,15,20-tetra(*p*-aminophenyl), porphyrin (H2TAPP), and 4,4′-biphenyldialdehyde under solvothermal conditions (Fig. 30). Palladium was decorated in the COF structure (Pd/H_2P-Bph-COF) by stirring a mixture of $Pd(OAc)_2$ and H_2P-Bph-COF in dichloromethane at room temperature (Table 2, entry 31). The Pd functionalized COF remained crystalline. The BET surface area, however, showed a significant drop from 550 to 147 $m^2\ g^{-1}$ for H_2P-Bph-COF and Pd/H_2P-Bph-COF, respectively. The catalytic activity of Pd/H_2P-Bph-COF was investigated in the Suzuki–Miyaura cross-coupling reaction at 110 °C in toluene (Table 1, entry 17). The results indicated a very efficient catalyst, and in the recycling test the catalyst worked as efficiently after the fourth cycle as in the first run and did not show any Pd leaching.[60]

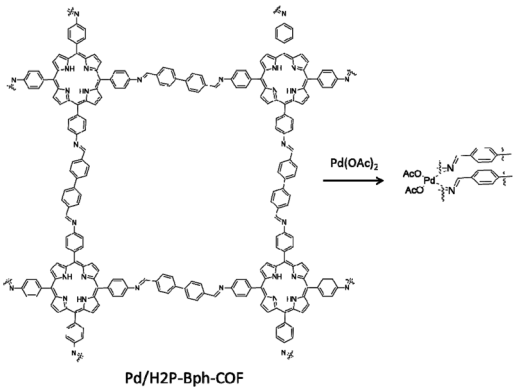

Fig. 30 Structure of Pd/H_2P-Bph-COF.

Bipyridine ligands have been employed by Chai and co-workers for coordinating palladium acetate. 2,2′-Bipyridine-5,5′-di-carbaldehyde (2,2′-BPyDCA) and 4,4′-biphenyldialdehyde with four different ratios (X = 25, 50, 75, 100%) were used to make COF by Schiff-base condensation with 4,4′,4″,4‴-(pyrene-1,3,6,8-tetrayl) tetraaniline (PyTTA) (Fig. 31a). The surface area calculated by BET analysis showed 538, 1554, 1438, and 1288 $m^2\ g^{-1}$, respectively, for the COFs and 283, 982, 847, and 731 $m^2\ g^{-1}$ for Pd@COFs. According to XPS analysis, both the imine and bipyridine show interaction with palladium (Fig. 31b).

The Pd@COFs possessed excellent catalytic activity in Heck coupling reactions, under N_2 atmosphere at 105 °C, resulting in high yields (70 to 96%) with the catalyst with 75% 2,2′-BPyDCA in the framework structure performing best.[61]

Gao *et al.* prepared a bimetallic catalyst by anchoring Mn and Pd in the framework of the Py-2,20-BPyPh COF. The host COF was prepared by condensation of PyTTA and 2,2′-bipyridine-5,5′-dicarbaldehyde (2,2′-BPyDCA) under solvothermal conditions at 120 °C for 3 days (Fig. 32a) (Table 2, entry 32).[62] Nitrogen sorption isotherms showed that the pore diameter of 2.6 nm did not change after Mn loading, however, after Pd loading the pore diameter decreased to 2.0 nm. Moreover, the BET surface area decreased from 2038 to 1711, and 1562 $m^2\ g^{-1}$ for Py-2,20-BPyPh COF, Mn@Py-2,20-BPyPh COF, and Mn/Pd@Py-2,20-BPyPh COF, respectively. The red-shift of Mn 2p, Pd 3d and blue-shift of N 1s peaks in XPS analysis proved the coordination of the metals with the nitrogens in the COF framework. The

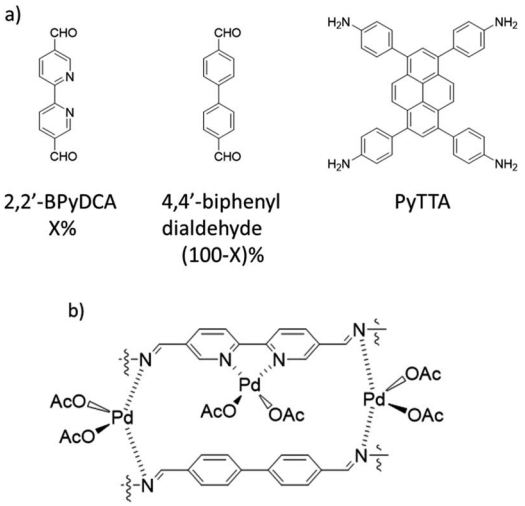

Fig. 31 (a) Linkers (b) coordination of palladium acetate with bipyridine and imine nitrogens.

control XPS analysis of Pd@2,20-BPyDCA Pd@BiPh COF confirmed that the Pd coordinated both with imine-nitrogen and bypyridine sites; in contrast, the Mn coordinates only with the bipyridine ligands.[63]

This catalyst was used as a heterogeneous catalyst for Heck coupling/epoxidation tandem reactions, with both steps of this reaction occurring in very high yield (95% and 98%) (Fig. 32b).

Stanley and co-workers prepared a palladium functionalized β-ketoenamine-linked TpBpy covalent organic framework by condensation of the 1,3,5-triformylphloroglucinol (Tp) and [2,2′-bipyridine]-5,5′-diamine (Bpy) followed by metalation with palladium acetate (Fig. 33). The prepared Pd@TpBpy was investigated as a heterogeneous catalyst in conjugate additions

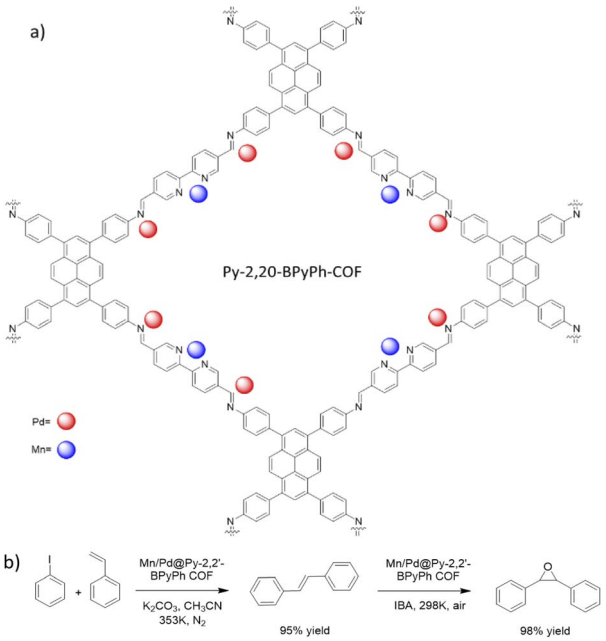

Fig. 32 (a) Structure of Py-2,20-BPyPh COF, (b) Heck coupling/epoxidation tandem reaction.

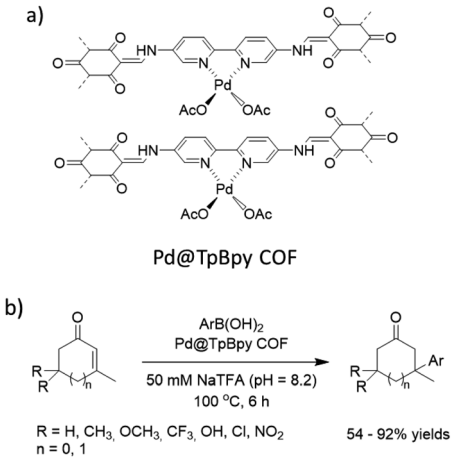

Fig. 33 (a) Structure of Pd@TpBpy COF, (b) conjugate additions of aryl boronic acids to β,β-disubstituted enones.

of aryl boronic acids to β,β-disubstituted enones in an aqueous NaTFA at 100 °C. The catalyst showed good to excellent yield for a wide scope of reactants. During recycling experiments the yield decreased from 99% to 79% after the seventh run, related to the decreased surface area and aggregation of palladium observed in the recycled catalyst.[64]

Ma *et al.* used a similar $Pd(OAc)_2$ functionalized TpBpyCOF and reduced the Pd to Pd NPs with $NaBH_4$ resulting in Pd-SJ04. The best surface area and pore volume were measured at 375 m^2 g^{-1} and 0.254 cm^3 g^{-1}, respectively. The prepared catalyst was used for the reductive amination of aldehydes, which showed excellent conversion and high selectivity for a wide range of reagents (Fig. 34).[65]

Palladium decorated COFs can also be synthesized using palladium coordinated building blocks, omitting the need for post-synthetic metalation. Banerjee and co-workers designed and synthesized Pd@TpBpy by condensation reaction of 1,3,5-triformylphloroglucinol (Tp) and 2,2′-bipyridine-5,5′-diamine palladium chloride (Bpy-$PdCl_2$) under solvothermal conditions (Table 2, entry 33). During the synthesis procedure, palladium nanoparticles are formed and immobilized in the crystalline structure of the COF. The palladium nanoparticles possessed a size of 12 ± 4 nm and were distributed uniformly over the COF matrix. Because of the bigger size of the nanoparticles compared to the pore size of the COF (2.3 nm), they spread around the surface and interlayer spaces.[66]

The catalytic activity of Pd@TpBpy was investigated in the synthesis of 2-arylbenzofuran and its derivatives (Fig. 35). A

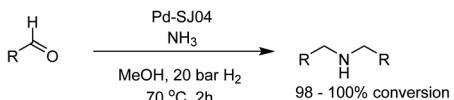

R = benzyl, 4-Cl-phenyl, 4-CH_3-phenyl, 4-methoxy-phenyl, 4-F-phenyl, 4-NH_2-phenyl, 4-CN-phenyl, 4-OH-phenyl, 4-ethoxy-phenyl, 3-Cl-phenyl, 3-OH-phenyl, 3-methoxy-phenyl, 3-F-phenyl, 3-CN-phenyl, 2-Cl-phenyl, 2-F-phenyl, 2-CH_3-phenyl, 2-methoxy-phenyl, Furyl, 2-CH_3-furyl, cyclohexyl, butyl, hexyl

Fig. 34 Reductive amination of aldehydes.

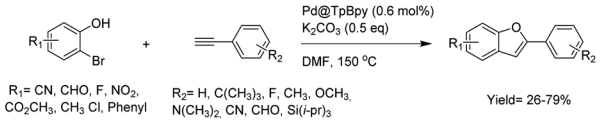

Fig. 35 Catalytic synthesis of 2-arylbenzofuran derivatives by Pd@TpBpy.

wide range of substitutions on 2-bromophenol and phenyl acetylene were explored with 26–79% yield. Also, the recycling procedure showed that the catalyst worked at least five times, but because of partial agglomeration of nanoparticles the yield slightly decreased (about 20%) after five runs.

Lin and co-workers also made another one Pd(II)/COF hybrid by using TpBpy-COF as a host for $PdCl_2$ to make Pd(II)@COF and used this material in conjugate additions of aryl boronic acids to α,β-unsaturated carboxylic acids (Fig. 36). To obtain high palladium loadings the catalyst was prepared by mechanochemical condensation of precoordinated Bpy-$PdCl_2$ with 1,3,5-triformylphloroglucinol (Tp). A range of β-arylated carboxylic acids could be synthesized using Pre-Pd(II)@COF as a catalyst, in medium to excellent yields (21 to 94%).[67]

In 2018 Dong *et al.* reported for the first time a COF-based chitosan aerogel that supported Pd NPs. The previously reported TpTe-1 COF was synthesized by condensation of terephthalohydrazide and 1,3,5-triformylphloroglucinol (Tp) and was used to immobilize Pd nanoparticles.[68] Pd@TpTe-1@chitosan aerogel is prepared under ultrasonic shaking followed by freeze-drying with chitosan and 1,4-butanediol diglycidyl ether cross-linker in an acidic solution. The prepared Pd@TpTe-1@chitosan aerogel has an elastic, sponge-like structure (Fig. 37) (Table 2, entry 34).[69]

The material showed excellent activity and stability for the dechlorination of a wide range of chlorophenols, in aqueous solution at room temperature, with ammonium formate as the hydrogen source, both in batch and in continuous-flow reactors.

Platero-Prats and co-workers studied the precise atomic structure of the Pd sites in imine and β-ketoenamine linked COFs. Archetypical imine and β-ketoenamine linked COFs were synthesized by condensation of 1,3,5-tris-(4-aminophenyl) benzene (TAPB) with 1,3,5 benzene-tricarbaldehyde (TAPB–BTCA COF) and 1,3,5-triformylphloroglucinol (TAPB–TFP COF) (Fig. 38). Two methods were used for the palladium incorporation. In the *in situ* method, the palladium precursor is added directly to the mixture of the COFs precursors. In the gel method the palladium precursors are added to the crystalline

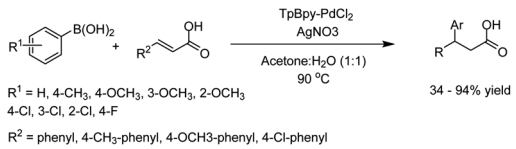

Fig. 36 Conjugate addition of aryl boronic acids to α,β-unsaturated carboxylic acids.

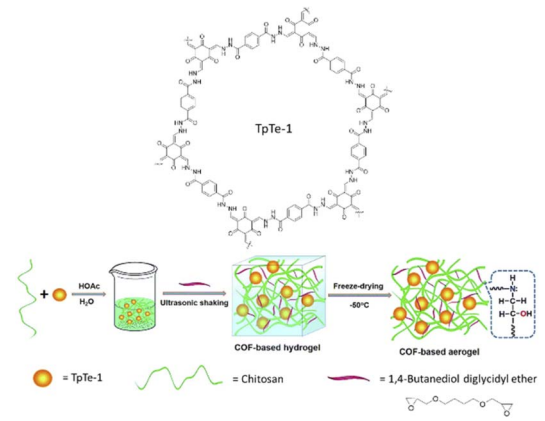

Fig. 37 Preparation of Pd@TpTe-1@chitosan aerogel (reproduced from ref. Dong *et al.*, *J. Mater. Chem. A*, 2018, **6**, 11140–11146 with permission from the Royal Society of Chemistry).

COF and the reaction is then continued in the oven. Importantly, using computational methods and synchrotron measurements, it became clear that for the imine linked TAPB–BTCA COF, local defect sites containing amines, formed by hydrolysis, are more active towards palladation than the pristine sites.

The metalation of TAPB–BTCA COF with the *in situ* method showed a decrease in surface area from 888 $m^2\ g^{-1}$ to 494 $m^2\ g^{-1}$ with Pd metalation. But interestingly, the surface area of BTCA–TFP COF increased from 550 $m^2\ g^{-1}$ to 664 $m^2\ g^{-1}$.[70]

The catalytic activity test in the Suzuki–Miyaura coupling reaction for all Pd/COFs catalysts showed good activity, but the *in situ* palladium-metalated imine-linked TAPB–BTCA catalyst worked better (Table 1, entry 13). TEM analysis of Pd/COFs showed Pd NPs with 4–15 nm particle sizes.

Pang *et al.* reported indazole containing β-ketoenamine and imine COFs as a host material for palladium nanoparticles by condensation of 1*H*-indazole-4,7-diamine (DAI) with 1,3,5-triformylphloroglucinol (TFP) (PdNPs@CON–DAI–TFP) and 1,3,5-

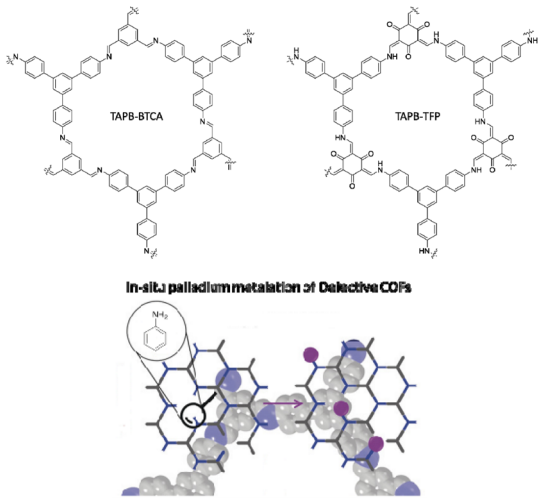

Fig. 38 Structure of TAPB–BTCA and TAPB–TFP COFs.

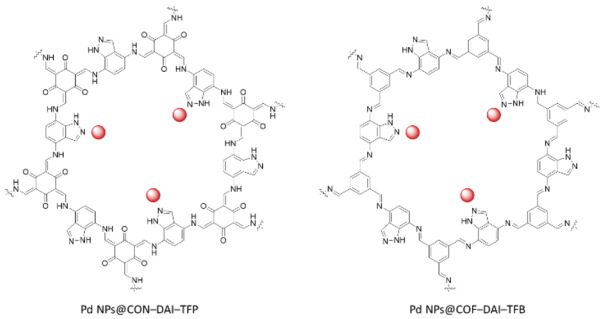

Fig. 39 Structure of Pd NPs@CON–DAI–TFP and Pd@COF–DAI–TFB.

triformylbenzene (TFB) (Fig. 39) (Table 2, entry 35). The structure of CON–DAI–TFP possessed a 2D slipped AA stacking layer with 1.8–5 nm height that included 5–14 layers and a surface area of 236 $m^2\ g^{-1}$. The HR-TEM of the β-ketoenamine linked Pd NPs@CON–DAI–TFP after impregnation of Pd and reduction by $NaBH_4$ revealed Pd nanoparticles with a narrow size distribution and a 1.74 nm average size, which is ten times smaller than the Pd nanoparticle size for the imine linked Pd@COF–DAI–TFB. The prepared CON–DAI–TFP-supported Pd-NPs exhibited excellent catalytic activity in reducing nitrophenol.[71]

Ji *et al.* synthesized COF-BTDH by condensing 1,3,5-triformylbenzene and 3,3′-dihydroxybenzidine and used it as support to coordinate $Pd(OAc)_2$ (Fig. 40a) (Table 2, entry 36). The material possessed pore sizes of 2–3 nm and 26 $m^2\ g^{-1}$ surface area.

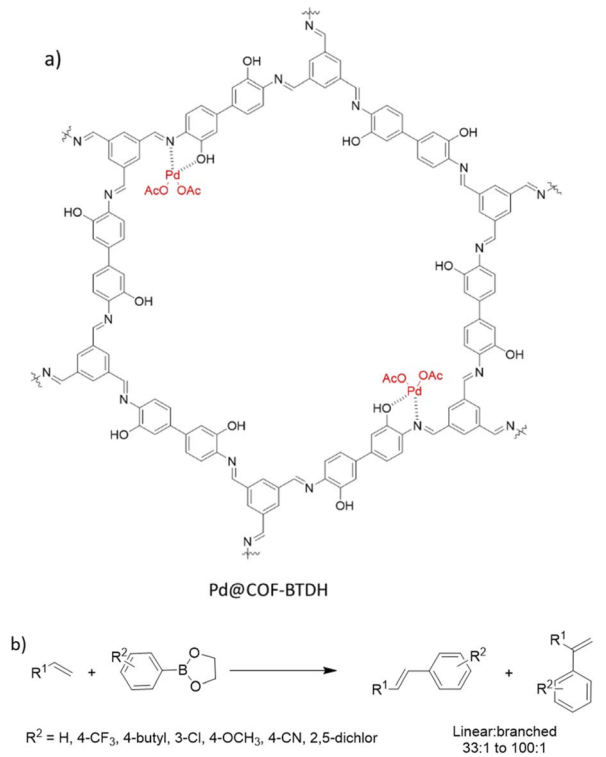

Fig. 40 (a) Structure of Pd@COF-BTDH (b) oxidative Heck coupling reaction.

Investigation of a wide scope of aliphatic alkenes proved the efficiency of Pd@COF-BTDH in the reaction with higher linear/branched products regioselectivity. DFT calculations for 1-octene showed a lower transition state energy for the linear product because of the coordination pattern and the ordered channels in the crystalline COF.[72]

Zhang and co-workers designed and developed phosphine-based COFs and used these for anchoring metal nanoparticles (Pd, Pt, Au) with controlled particle sizes. Phos-COF-1 was synthesized by solvothermal condensation of tri-(4-formylphenyl)phosphine and *p*-phenylenediamine (Fig. 41) (Table 2, entry 37). The resulting Phos-COF-1 possessed a surface area of 818 $m^2\ g^{-1}$ and a pore size of 1.56 nm. According to the XRD spectra, the material possessed a eclipsed AA stacking and staggered ABC stacking crystals.[73]

The PdNPs@Phos-COF-1 was prepared by suspension of K_2PdCl_4 and the COF in methanol and reduction with $NaBH_4$. The prepared nanoparticles have 1.62 ± 0.37 nm diameters and are well-dispersed in the framework. The main reason for these tuned NP sizes is the orderly distribution of PPh_3 functional groups in the porous lattice and the growth of NPs inside the pores.

The catalytic activity of the PdNPs@Phos-COF-1 was investigated in the Suzuki coupling reaction in DMF/water at 50 °C (Table 1, entry 14). These ultrafine PdNPs showed excellent activity and stability in comparison to the commercially available Pd sources such as $Pd(PPh_3)_2Cl_2$, $Pd_2(dba)_3$, and Pd/C.

The Phos-COF-1 is also used for ultrafine PtNPs@Phos-COF-1 and AuNPs@Phos-COF-1 with the same method. The products showed excellent catalytic activity in nitroarenes reduction.

Bachas and co-workers designed a photocatalytic hybrid metal catalyst by loading Pd NPs/COF on the surface of Cu_2O cubes (Fig. 42). ACOF-1 was synthesized by condensation of 1,3,5-triformylbenzene and hydrazine hydrate under solvothermal conditions. To load the prepared ACOF-1 on the surface of Cu_2O, the COF was dispersed in a copper sulfate solution in the presence of polyvinylpyrrolidone, sodium carbonate, sodium citrate and were kept at 80 °C in the

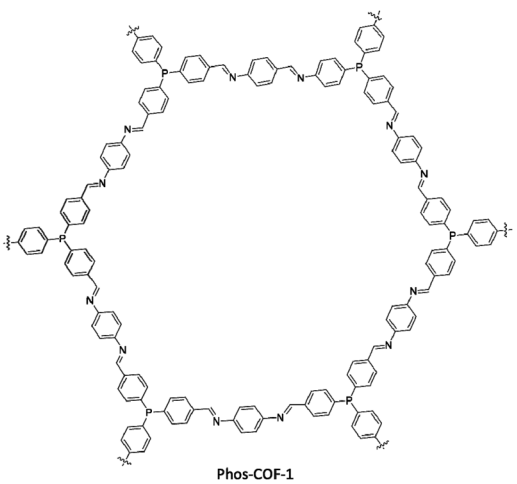

Fig. 41 Structure of Phos-COF-1.

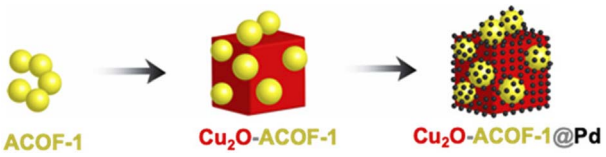

Fig. 42 Structure of Cu_2O-ACOF-1@Pd (reproduced from ref. Bachas *et al., ACS Appl. Nano Mater.*, 2021, **4**, 2795–2805 copyright 2021, American Chemical Society).

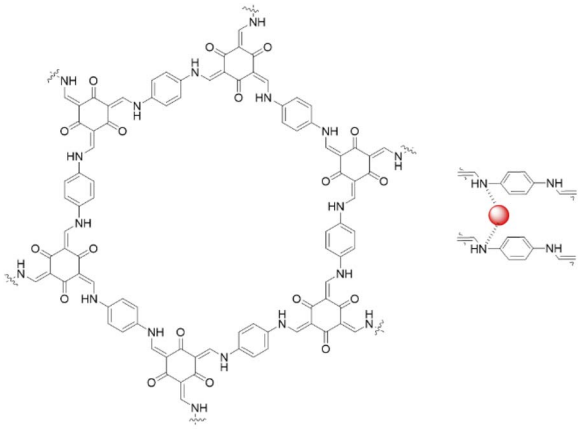

Fig. 43 Structure of COF-SMC2 and Pd@COF-SMC2.

darkness (Cu_2O-ACOF-1). The prepared precipitates was dispersed in an ethanolic solution of palladium acetate and stirred overnight in darkness to prepare Cu_2O-ACOF-1@Pd. The BET surface area of ACOF-1, Cu_2O-ACOF-1, and Cu_2O-ACOF-1@Pd are 1134, 114, and 98 $m^2\ g^{-1}$, respectively. This catalyst showed outstanding photocatalytic activity for the degradation of polychlorinated biphenyls (PCBs).[74]

Ma and co-workers fabricated four different COFs based on Schiff-base reaction of 1,3,5-triformylphloroglucinol with 2,2′-bipyridine-5,5′-diamine (COF-SMC1), *p*-phenylenediamine (COF-SMC2), 4,4′-diaminobiphenyl (COF-SMC3), and 1,3,5-triformylbenzene with 2,2′-bipyridine-5,5′-diamine (COF-SMC4). They coordinated the COFs with $Pd(OAc)_2$ by stirring in DCM (Table 2, entry 38). XPS analysis showed, besides the main peaks of Pd^{2+}, two small peaks of Pd^0, that were hypothesized to be caused by electron donating of imine groups during the incorporation process. TEM images showed Pd uniformly dispersed in the COFs matrix with a 5 nm average particle size. The BET analysis showed a dramatical decrease in the surface area from 363 to 24 $m^2\ g^{-1}$, related to the presence of Pd nanoparticles.[75]

The COF-SMC2 was explored as an excellent heterogeneous catalyst the Suzuki–Miyaura coupling reaction for a wide range of reagents in ethanol at 80 °C. Notably, it is also able to synthesize halo-substituted biaryl products, avoiding homo-couplings of halogenated aryl boronic acids (Table 1, entry 15) (Fig. 43).

Alemán and coworkers prepared an imine-based covalent organic framework, including a phenanthroline unit (Phen-COF) as a ligand for Pd binding (Pd@Phen-COF) (Table 2,

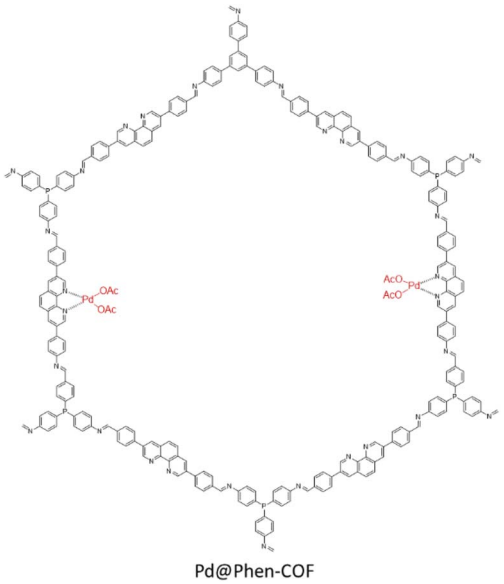

Fig. 44 Structure of Pd@Phen-COF.

entry 39). The BET surface area slightly decreased from 482 to 447 $m^2\ g^{-1}$ after palladium decoration. XPS analysis of the Pd@Phen-COF for the Pd and N atoms showed a +2 oxidation state for palladium which is in accordance with the model complex of $[Pd(phen)(OAc)_2]$, and a shift in pyridinic nitrogens from 98.8 to 398.0 eV that proved the coordination of Pd with phenanthroline (Fig. 44).[76]

The catalytic investigation of the Pd@Phen-COF showed excellent activity (80 to 99% yields) in the Suzuki–Miyaura coupling reactions in iPrOH : H_2O (4 : 1) at room temperature (Table 1, entry 16). Also, the recycling process proved the very high stability for the catalyst, and ICP analysis showed no Pd leaching during the reaction.

Yang *et al.* synthesized a Pd NPs/COF hybrid based on imine-linked TB-COF by condensation of 1,3,5-tris(*p*-formylphenyl) benzene and benzidine (Fig. 45). Loading of Pd NPs was done using Na_2PdCl_4 and reduction with H_2 gas. The morphology of the Pd*x*/TB-COF with different percentages (x = 1.4–5 wt%) of Pd showed well-dispersed nanoparticles with a 1.8 nm average size. The small particle sizes of Pd related to the well-ordered pore structure and the large amounts of imine groups.

Catalytic hydrogenation reaction of nitroarenes was investigated by the Pd1.4/TB-COF under H_2 atmosphere with excellent conversion and selectivity. The recycling test of Pd1.4/TB-COF showed no aggregation of Pd NPs and no noticeable decrease in conversion after six runs.[77]

Fu and co-workers used a COF–carbon nanotube nanocomposite (CNT–COF) to stabilize ultrafine Pd NPs with narrow sizes (Fig. 46). They fabricated the CNT–COF based on the *in situ* growth of an imine-based COF by condensation of 1,3,6,8-tetrakis(*p*-formylphenyl)pyrene (TFPPy), and *p*-phenylenediamine on the surface of the CNT (Table 2, entry 40). Then, palladium was loaded on the CNT–COF nanocomposite and reduced by $NaBH_4$ to prepare the CNT–COF–Pd. The prepared catalyst has a 975 $m^2\ g^{-1}$ surface area and hosts Pd NPs with 2.8 nm particle

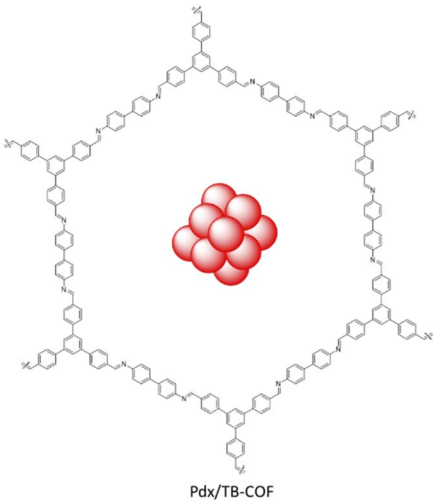

Fig. 45 Structure of Pd*x*/TB-COF.

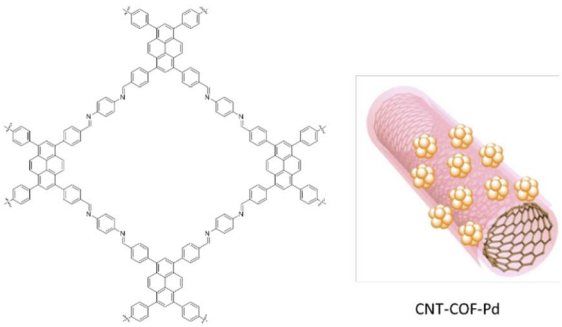

Fig. 46 Structure of CNT–COF–Pd (reproduced from ref. Fu *et al.*, *ACS Appl. Nano Mater.*, 2022, **5**, 597–604 copyright 2022, American Chemical Society).

sizes. The CNT–COF–Pd composite showed excellent activity for electrocatalytic ethanol oxidation.[78]

2.6 3D-COFs

In 2012 a 3D COF was used for the first time, by Fisher and co-workers, as a host for Pd NPs (Pd@COF-102) (Fig. 47). They studied the hydrogen storage capacities with different percentages of Pd impregnation as organic–inorganic hybrid material. The 3D COF-102 was synthesized by self-condensing tetra(4-dihydroxyboryl phenyl)methane (TBPM).[79] The hydrogen capacity of COF-102 was optimized by the selective decoration of the interior surface of the COF with varying amounts of Pd nanoparticles (30, 20, 9.5, and 3.5 wt%). As a palladium nanoparticle precursor [Pd(η^3-C_3H_5) (η^5-C_5H_5)] was used, which has the appropriate size to infiltrate the pores of the framework easily (Table 2, entry 41). Approximately 2.5 nm-sized Pd nanoparticles were made under UV-light irradiation at room temperature. The crystalline structure of the host COF remained unchanged, but the surface area decreased, from 3145 $m^2\ g^{-1}$ for 3.5 wt% to 1419 for 30 wt% palladium, due to the filling of the pores of the framework with the Pd

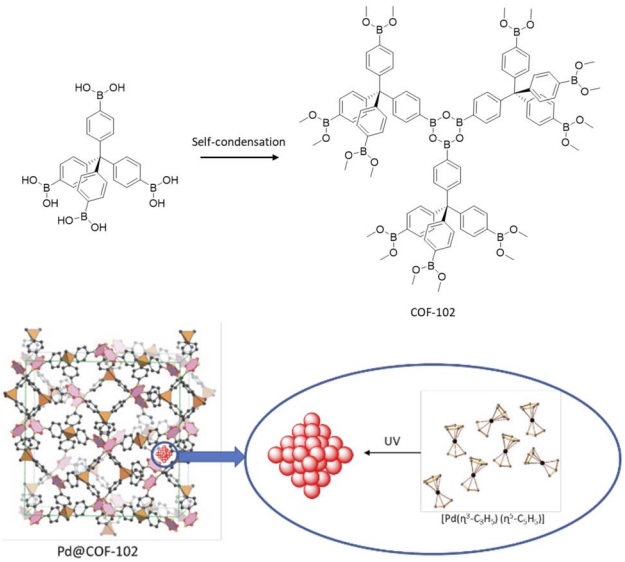

Fig. 47 Structures of COF-102 and Pd@COF-102.

nanoparticles. The authors found that even though the hydrogen uptake of Pd@COF-102 was slightly reduced at 77 K, at 298 K, the hydrogen capacity increased 2–3 times in comparison to the host COF.[80]

Imine-linked 3D COF-300, prepared by the condensation of tetrahedral tetra-(4-anilyl)-methane and linear terephthaldehyde building blocks,[81] was used for stabilization of $Pd(OAc)_2$ by Esteves and co-workers (Fig. 48) (Table 2, entry 42).[82]

The palladium-hybrid COF was prepared by refluxing $Pd(OAc)_2$ and COF-300 in dichloromethane. The crystallinity studies of the final catalyst did not show any difference with the host COF, which proves the structure stayed intact during the impregnation procedure. However, the surface area dropped significantly from 1373 $m^2\ g^{-1}$ to 270 $m^2\ g^{-1}$ due to the occupation of pores with $Pd(OAc)_2$. The positive shift of the binding energy for the N 1s region in XPS analysis proved the strong Pd–N interaction.

The catalytic activity evaluation of $Pd(OAc)_2$@COF-300 was performed by Suzuki–Miyaura cross-coupling reaction for a wide variety of aryl halide and boronic acids in MeOH/H_2O at 70 °C with 0.1 mol% Pd with 26% to 100% yields (Table 1, entry 18). Moreover, the application of the catalyst in a continuous flow coupling reaction of bromobenzene and phenylboronic acid showed that it has a high stability and selectivity for this

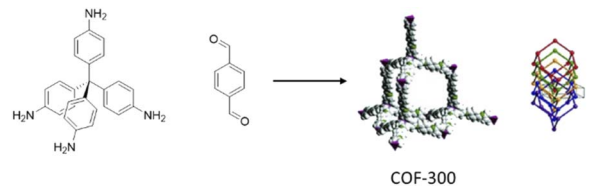

Fig. 48 Schematic structure of COF-300.

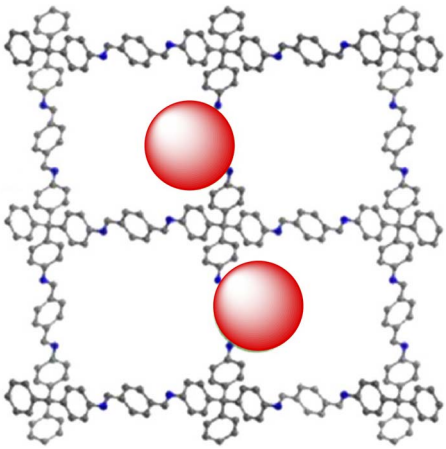

Fig. 49 Structure of COF-300-1114.

reaction. Also, this catalyst possessed high efficiency in the Heck and Sonogashira coupling reaction.

Yue and coworkers used a non-stoichiometric synthon strategy (NSS) to synthesize a COF with extra, unreacted amine functional groups to confine metal nanoparticles. The authors used tetrakis(4-anilyl)methane (TAM) and terephthaldehyde (TPA) building blocks in a non-stoichiometric ratio to make COF-300-*xy* where *x* and *y* are the numerator and denominator of the ratio for TAM and TPA, respectively. COF-300-1114 has the same crystallinity as COF-300, but possessed unreacted amine groups in the structure. The palladium nanoparticles have an extremely small (1.58 nm) and well-dispersed structure after the palladium impregnation and reduction procedure (Fig. 49).[83]

The catalytic activity of COF-300-1114 was investigated in the selective oxidation of benzyl alcohol to benzaldehyde. The reaction under 0.1 MPa of O_2 at 90 °C in toluene showed low to excellent yield and selectivity, for different reactants.

Zhao and co-workers designed a new 3D COF and used it as a Pd-based heterogeneous catalyst. 9,9′-Spirobi[fluorene]-3,3′,6,6′-tetraamine and [3,3′-bipyridine]-6,6′-dicarbaldehyde were used as linkers to make the SP-3D-COF-BPY as a 3D COF under solvothermal conditions. The orthogonal structure of SP caused the COF to possess rigid and unobstructed tetragonal-disphenoid diamond (dia) channels and a surface area of 1945 $m^2\ g^{-1}$.

Palladium loading was done by stirring the COF and palladium acetate in dichloromethane (Pd(II)@SP-3D-COF-BPY) followed by reduction with $NaBH_4$ (PdNP@SP-3D-COF-BPY) (Fig. 50) (Table 2, entry 43). The catalytic activity of these two structures investigated in the Suzuki–Miyaura coupling reactions and Pd(II)@SP-3D-COF-BPY showed a higher activity in *p*-xylene at 70 °C (Table 1, entry 19).[84]

Zhao *et al.* reported an ultrafine Pd NPs/COF hybrid based on a TPM-3D-COF-BPY substrate. The COF was fabricated by condensation of tetra(4-aminophenyl)methane and [2,2′-bipyridine]-5,5′-dicarboxaldehyde under solvothermal conditions at 120 °C (Table 2, entry 44). The product has a 955.56 $m^2\ g^{-1}$ surface area and 1.17 nm pore size. The Pd(II) impregnation and

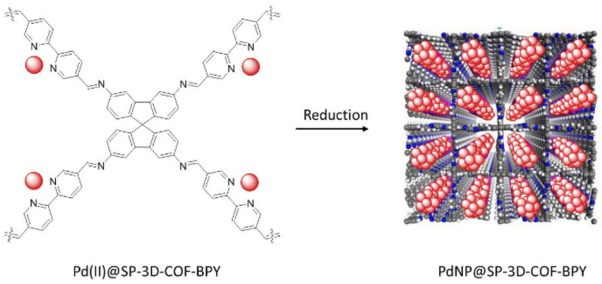

Fig. 50 Structures of Pd(II)@SP-3D-COF-BPY and PdNP@SP-3D-COF-BPY.

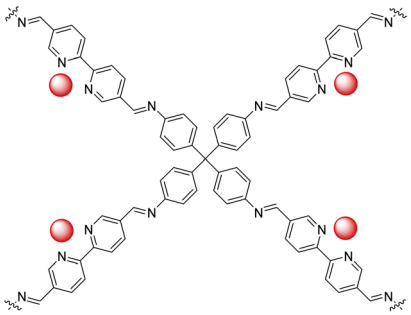

Fig. 51 Structure of Pd@TPM-3D-COF-BPY.

reduction was done by a physical mixture of the COF and K_2PdCl_4, followed by reduction with $NaBH_4$. The TEM image of Pd@TPM-3D-COF-BPY showed Pd NPs with an average size of 1.12 nm in diameter (Fig. 51).[85]

The catalytic activity of the product was explored by The Suzuki–Miyaura coupling reaction in aqueous solution at 70 °C with high yields (45–99%) (Table 1, entry 20).

2.7 The Suzuki–Miyaura cross coupling reaction

Since the discovery of the Suzuki–Miyaura cross-coupling reaction in 1979, it has become one of the important methods to construct a carbon–carbon bonds by coupling of an organoboron species and aryl halide in the presence of a catalytic amount of nickel or palladium.[86] The main advantages of this method that make it an essential tool in the synthesis of natural and pharmaceutical products are the mild reaction conditions and the stable, commercially available, and environmentally benign boronic acids.[87]

During the last decades, a lot of effort have been made to improve the catalysts' efficiency and to use more eco-friendly conditions for this reaction.[88]

As mentioned in the previous parts, COFs are used as one of the important hosts to stabilize palladium. The Suzuki–Miyaura coupling reaction is one of the main reactions used to investigate the catalytic activity of prepared Pd/COFs hybrids. The catalytic activity of all discussed catalysts was compared in cross-coupling of bromobenzene and phenylboronic acid and is summarized in Table 1.

Palladium was anchored in both the +2 oxidation state or as metallic nanoparticles on the COFs. The highest efficiency was

observed for Pd@COF-NHC (Table 1, entry 11), which was prepared by immobilization of palladium nanoparticles in a NHC-functionalized COF. The reaction was done in neat water, room temperature, and short reaction time for aryl iodides and bromides. Also, $Pd(OAc)_2$@COF-300 showed high activity in MeOH/H_2O, at 70 °C and 20 minutes with a 100% conversion (Table 1, entry 17). Some other catalysts worked in neat water with good activity (Table 1, entry 3, 8, 9, 11, and 12). Pd@COF-TM, as one of them (Table 1, entry 8), showed high activity for aryl chloride with high yields (55 to 95%), in neat water and room temperature. Even though all of the catalysts are stable in the reaction process, the PdNPs@Thio-COF could keep the ultrafine structure of palladium nanoparticles after recycling, and ultimately prevent aggregation of Pd NPs (Table 1, entry 10).

2.8 Reduction of nitroarenes

Aromatic amines are important group of organic compounds that used as key precursors for a wide range of pharmaceuticals products, dyes, polymers and *etc.* The catalytic reduction of nitroarenes to aromatic amines is the most extensively studied method for synthesis of them. Also, because of identification of nitroarenes as toxic and carcinogenic compounds removal of them from aqueous media is a challenge.

In this review, some different Pd/COFs that were synthesised and used for this purpose are covered. Pd@NHCS as the first Pd/COFs that reported for reduction nitrobenzene, showed very high activity. The reaction showed 88% conversion within only 50 minutes, under an atmosphere pressure of H_2 at 25 °C. Pd@CTF as an triazine based catalyst was used for reduction a wide range of nitroarenes in the presence formic acid/ammonium formate in aqueous ethanol at room temperature. More than 99% conversion and selectivity for nitrobenzene in 0.2 h, indicate highly promising catalyst for this goal.

Moreover, reduction of nitrophenol with Pd@H-TpPa catalyst by using $NaBH_4$ as reducing agent showed >99% conversion in just 4 minutes. Pd@COF-BPh also used as a catalyst for reduction a wide range of nitroarenes by $NaBH_4$ as reducing agent, that most of them showed >99% conversion in a few minutes.

As explained previously Pd@H-PPA was used as a catalyst for hydrogenation of nitroarenes by using ammonia borane as the source of hydrogen. >99% conversion in 2 minutes make it very efficient catalyst for this type of reaction.

2.9 Dechlorination

Arylchlorides because of their high toxicity and poor biodegradability are categorized in dangerous materials to the environment. Therefore, developing stable catalyst for dechlorination of this compounds are very essential; although, the high stability of carbon–chlorine bond is the main challenge of this conversion.

The catalytic activity of Pd/NCN explored for hydrodechlorination of chlorophenols. They found excellent conversion of chlophenol to phenol at room temperature and atmosphere pressure of H_2; by increasing temperature to 80 °C, cyclohexanone is synthesised with >99% conversion and selectivity. Also, Pd@TpTe-1@chitosan aerogel is used for dichlorination of arylchlorides in continues flow reactor at room temperature in the presence of HCO_2NH_4 in aqueous solution with excellent conversions. The researchers found that the COFs as the host of Pd show much higher activity for these reactions.

Moreover, Pd@COF/NFC composite membrane is used in dechlorination of *ortho*-dichlorobenzene by using $NaBH_4$ with 90% conversion at room temperature and 105 minutes.

3 Conclusions

The COFs have significant potential and advantages to be considered as an alternative solid support to immobilize palladium as metal complexes or as nanoparticles with high stability and recyclability. The tuneable and designable pore size of the COFs can be adjusted to be a host for different size nano particles, and the permanent mesoporous structure of COFs prevent the agglomeration and deactivation of the catalyst. Also, because of the permanent and designable pore size of the COFs, they could increase the selectivity for certain products in the reaction procedure.

Especially, functionalized COFs are an interesting group of materials for synthesizing ultrafine nanoparticles as the functional groups can work as a surfactant to control the growth of the nanoparticles. Also, strong interaction between the COFs and the nanoparticles could keep the uniform dispersion of NPs and prevent agglomeration during the recycling procedure.

This review was an overview of reported palladium immobilized COFs and their catalytic activity that increased exponentially during the last ten years. It looks like COFs will be playing an essential role in the future of Pa catalysed reactions.

Conflicts of interest

There are no conflicts to declare.

Acknowledgements

The authors acknowledge the Research Board of Ghent University (BOF GOA20177000303) for funding.

Notes and references

1 M. Pagliaro, V. Pandarus, R. Ciriminna, F. Béland and P. DemmaCarà, *ChemCatChem*, 2012, **4**, 432–445.
2 P. Ruiz-Castillo and S. L. Buchwald, *Chem. Rev.*, 2016, **116**, 12564–12649.
3 G. Zeni and R. C. Larock, *Chem. Rev.*, 2006, **106**, 4644–4680.
4 Q. A. Chen, Z. S. Ye, Y. Duan and Y. G. Zhou, *Chem. Soc. Rev.*, 2013, **42**, 497–511.
5 D. S. Surry and S. L. Buchwald, *Angew. Chem., Int. Ed.*, 2008, **47**, 6338–6361.
6 G. C. Fortman and S. P. Nolan, *Chem. Soc. Rev.*, 2011, **40**, 5151–5169.
7 L. Yin and J. Liebscher, *Chem. Rev.*, 2007, **107**, 133–173.

8 H. Hagiwara, Y. Shimizu, T. Hoshi, T. Suzuki, M. Ando, K. Ohkubo and C. Yokoyama, *Tetrahedron Lett.*, 2001, **42**, 4349–4351.
9 M. L. Toebes, J. A. Van Dillen and K. P. De Jong, *J. Mol. Catal. A: Chem.*, 2001, **173**, 75–98.
10 A. Kumbhar, *Top. Curr. Chem.*, 2017, **375**, 1–28.
11 Q. Yang, F. Yao, Y. Zhong, F. Chen, X. Shu, J. Sun, L. He, B. Wu, K. Hou, D. Wang and X. Li, *Part. Part. Syst. Charact.*, 2019, **36**, 1–19.
12 V. Polshettiwar, C. Len and A. Fihri, *Coord. Chem. Rev.*, 2009, **253**, 2599–2626.
13 L. Li, H. Zhao and R. Wang, *ACS Catal.*, 2015, **5**, 948–955.
14 C. E. Chan-Thaw, A. Villa, P. Katekomol, D. Su, A. Thomas and L. Prati, *Nano Lett.*, 2010, **10**, 537–541.
15 C. S. Diercks and O. M. Yaghi, *Science*, 2017, **355**, eaal1585.
16 S. B. Kalidindi and R. A. Fischer, *Phys. Status Solidi B*, 2013, **250**, 1119–1127.
17 Y. Zeng, R. Zou and Y. Zhao, *Adv. Mater.*, 2016, **28**, 2855–2873.
18 M. Dogru and T. Bein, *Chem. Commun.*, 2014, **50**, 5531–5546.
19 J. You, Y. Zhao, L. Wang and W. Bao, *J. Cleaner Prod.*, 2021, **291**, 125822.
20 Y. Yusran, Q. Fang and V. Valtchev, *Adv. Mater.*, 2020, **32**, 1–27.
21 S. Wang, X. Xu, Y. Yue, K. Yu, Q. Shui, N. Huang and H. Chen, *Small Struct.*, 2020, **1**, 2000021.
22 M. S. Lohse and T. Bein, *Adv. Funct. Mater.*, 2018, **28**, 1705553.
23 S. Y. Ding, J. Gao, Q. Wang, Y. Zhang, W. G. Song, C. Y. Su and W. Wang, *J. Am. Chem. Soc.*, 2011, **133**, 19816–19822.
24 L. Chen, L. Zhang, Z. Chen, H. Liu, R. Luque and Y. Li, *Chem. Sci.*, 2016, **7**, 6015–6020.
25 D. Sun, S. Jang, S. J. Yim, L. Ye and D. P. Kim, *Adv. Funct. Mater.*, 2018, **28**, 1707110.
26 X. Yang, Y. He, L. Li, J. Shen, J. Huang, L. Li, Z. Zhuang, J. Bi and Y. Yu, *Chem.–Eur. J.*, 2020, **26**, 1864–1870.
27 S. Hao, S. Li and Z. Jia, *J. Nanopart. Res.*, 2020, **22**, 1–10.
28 P. Sun, J. Hai, S. Sun, S. Lu, S. Liu, H. Liu, F. Chen and B. Wang, *Nanoscale*, 2020, **12**, 825–831.
29 S. Kandambeth, A. Mallick, B. Lukose, M. V. Mane, T. Heine and R. Banerjee, *J. Am. Chem. Soc.*, 2012, **134**, 19524–19527.
30 P. Pachfule, M. K. Panda, S. Kandambeth, S. M. Shivaprasad, D. D. Díaz and R. Banerjee, *J. Mater. Chem. A*, 2014, **2**, 7944–7952.
31 S. Y. Ding, P. L. Wang, G. L. Yin, X. Zhang and G. Lu, *Int. J. Hydrogen Energy*, 2019, **44**, 11872–11876.
32 K. Cui, W. Zhong, L. Li, Z. Zhuang, L. Li, J. Bi and Y. Yu, *Small*, 2019, **15**, 1–8.
33 Y. Li, B. Pei, J. Chen, S. Bing, L. Hou, Q. Sun, G. Xu, Z. Yao and L. Zhang, *J. Colloid Interface Sci.*, 2021, **591**, 273–280.
34 R. Chen, F. Wang, J. Zhang, Y. Shao, H. Jiang and Y. Liu, *Ind. Eng. Chem. Res.*, 2020, **59**, 18489–18499.
35 X. Wan, X. Wang, G. Chen, C. Guo and B. Zhang, *Mater. Chem. Phys.*, 2020, **246**, 122574.
36 H. Jiang, X. Shen, F. Wang, J. Zhang, Y. Du and R. Chen, *Ind. Eng. Chem. Res.*, 2021, **60**, 13523–13533.
37 H. C. Ma, J. L. Kan, G. J. Chen, C. X. Chen and Y. Bin Dong, *Chem. Mater.*, 2017, **29**, 6518–6524.
38 S. Lin, Y. Hou, X. Deng, H. Wang, S. Sun and X. Zhang, *RSC Adv.*, 2015, **5**, 41017–41024.
39 D. Mullangi, S. Nandi, S. Shalini, S. Sreedhala, C. P. Vinod and R. Vaidhyanathan, *Sci. Rep.*, 2015, **5**, 1–12.
40 V. Sadhasivam, R. Balasaravanan, C. Chithiraikumar and A. Siva, *ChemistrySelect*, 2017, **2**, 1063–1070.
41 D. Kaleeswaran, R. Antony, A. Sharma, A. Malani and R. Murugavel, *Chempluschem*, 2017, **82**, 1253–1265.
42 M. Fan, Y. Long, Y. Zhu, X. Hu and Z. Dong, *Appl. Catal., A*, 2018, **568**, 130–138.
43 J. Li, L. Zhang, X. Liu, N. Shang, S. Gao, C. Feng, C. Wang and Z. Wang, *New J. Chem.*, 2018, **42**, 9684–9689.
44 V. Sadhasivam, M. Mathappan, M. Harikrishnan, C. Chithiraikumar, S. Murugesan and A. Siva, *Res. Chem. Intermed.*, 2018, **44**, 2853–2866.
45 M. Fan, W. D. Wang, Y. Zhu, X. Sun, F. Zhang and Z. Dong, *Appl. Catal., B*, 2019, **257**, 117942.
46 P. Puthiaraj, K. Yu, S. E. Shim and W. S. Ahn, *Mol. Catal.*, 2019, **473**, 110395.
47 Y. X. Chen, S. Zhang, Y. J. Xue, L. P. Mo and Z. H. Zhang, *Appl. Organomet. Chem.*, 2021, 1–15.
48 F. Haase, E. Troschke, G. Savasci, T. Banerjee, V. Duppel, S. Dörfler, M. M. J. Grundei, A. M. Burow, C. Ochsenfeld, S. Kaskel and B. V. Lotsch, *Nat. Commun.*, 2018, **9**, 2600.
49 Y. Yang, H. Niu, W. Zhao, L. Xu, H. Zhang and Y. Cai, *RSC Adv.*, 2020, **10**, 29402–29407.
50 S. Wu, N. Ding, P. Jiang, L. Wu, Q. Feng, L. Zhao, Y. Wang, Q. Su, H. Zhang and Q. Yang, *Tetrahedron Lett.*, 2020, **61**, 152656.
51 S. Wu, Y. Zhang, H. Jiang, L. Wu, N. Ding, P. Jiang, H. Zhang, L. Zhao, F. Yin and Q. Yang, *Tetrahedron*, 2020, **76**, 131664.
52 Z. Dong, H. Pan, P. Gao, Y. Xiao, L. Fan, J. Chen and W. Wang, *Catal. Lett.*, 2022, **152**, 299–306.
53 H. Zhu, W. David Wang, F. Li, X. Sun, B. Li, Q. Song, J. Kou, K. Ma, X. Ren and Z. Dong, *J. Colloid Interface Sci.*, 2022, **606**, 1340–1351.
54 S. Lu, Y. Hu, S. Wan, R. McCaffrey, Y. Jin, H. Gu and W. Zhang, *J. Am. Chem. Soc.*, 2017, **139**, 17082–17088.
55 B. J. Yao, J. T. Li, N. Huang, J. L. Kan, L. Qiao, L. G. Ding, F. Li and Y. Bin Dong, *ACS Appl. Mater. Interfaces*, 2018, **10**, 20448–20457.
56 J. Yang, Y. Wu, X. Wu, W. Liu, Y. Wang and J. Wang, *Green Chem.*, 2019, **21**, 5267–5273.
57 J. H. Li, Z. W. Yu, Z. Gao, J. Q. Li, Y. Tao, Y. X. Xiao, W. H. Yin, Y. L. Fan, C. Jiang, L. J. Sun and F. Luo, *Inorg. Chem.*, 2019, **58**, 10829–10836.
58 J. C. Wang, C. X. Liu, X. Kan, X. W. Wu, J. L. Kan and Y. Bin Dong, *Green Chem.*, 2020, **22**, 1150–1155.
59 X. Yang, Y.-R. Du, P.-X. Guan, H.-Y. Liu, Y.-F. Wang and B.-H. Xu, *ChemCatChem*, 2022, **14**, e202101594.
60 Y. Hou, X. Zhang, J. Sun, S. Lin, D. Qi, R. Hong, D. Li, X. Xiao and J. Jiang, *Microporous Mesoporous Mater.*, 2015, **214**, 108–114.
61 J. Zhang, Y. Peng, W. Leng, Y. Gao, F. Xu and J. Chai, *Chin. J. Catal.*, 2016, **37**, 468–475.

62 C. Xiong, H. Ning, G. Jia, X. Hong, X. Fei and J. Donglin, *Chem. Commun.*, 2014, **50**, 6161–6163.
63 W. Leng, R. Ge, B. Dong, C. Wang and Y. Gao, *RSC Adv.*, 2016, **6**, 37403–37406.
64 P. M. Heintz, B. P. Schumacher, M. Chen, W. Huang and L. M. Stanley, *ChemCatChem*, 2019, **11**, 4286–4290.
65 J. Liu, M. Zhang and L. Ma, *Catalysts*, 2021, **11**, 1–14.
66 M. Bhadra, H. S. Sasmal, A. Basu, S. P. Midya, S. Kandambeth, P. Pachfule, E. Balaraman and R. Banerjee, *ACS Appl. Mater. Interfaces*, 2017, **9**, 13785–13792.
67 M. Wen, S. Lu, C. Fan, K. Shen, S. Lin and Q. Pan, *Appl. Organomet. Chem.*, 2021, **35**, e6263.
68 W. Zhang, P. Jiang, Y. Wang, J. Zhang, Y. Gao and P. Zhang, *RSC Adv.*, 2014, **4**, 51544–51547.
69 F. Li, L. G. Ding, B. J. Yao, N. Huang, J. T. Li, Q. J. Fu and Y. Bin Dong, *J. Mater. Chem. A*, 2018, **6**, 11140–11146.
70 I. Romero-Muñiz, A. Mavrandonakis, P. Albacete, A. Vega, V. Briois, F. Zamora and A. E. Platero-Prats, *Angew. Chem.*, 2020, **132**, 13113–13120.
71 F. Lu, Y. Li, Q. Shi, C. Zhao, S. Li and S. Pang, *New J. Chem.*, 2020, **44**, 15354–15361.
72 J. Han, X. Sun, X. Wang, Q. Wang, S. Hou, X. Song, Y. Wei, R. Wang and W. Ji, *Org. Lett.*, 2020, **22**, 1480–1484.
73 R. Tao, X. Shen, Y. Hu, K. Kang, Y. Zheng, S. Luo, S. Yang, W. Li, S. Lu, Y. Jin, L. Qiu and W. Zhang, *Small*, 2020, **16**, 1–8.
74 A. E. Elmetwally, E. Zeynaloo, D. Shukla, B. Surnar, S. Dhar, J. L. Cohn, M. R. Knecht and L. G. Bachas, *ACS Appl. Nano Mater.*, 2021, **4**, 2795–2805.
75 J. Liu, H. Zhan, N. Wang, Y. Song, C. Wang, X. Wang, L. Ma and L. Chen, *ACS Appl. Nano Mater.*, 2021, **4**, 6239–6249.
76 A. López-Magano, R. Mas-Ballesté and J. Alemán, *Adv. Sustainable Syst.*, 2021, 2100409.
77 C. Li, X. Ren, M. Guo, W. Li, H. Li and Q. Yang, *Catal. Sci. Technol.*, 2021, **11**, 3873–3879.
78 X. Tan, R. Wu, Q. Zhu, Q. Gou, Y. Zhang, H. Huang and L. Fu, *ACS Appl. Nano Mater.*, 2022, **5**, 597–604.
79 G. V Knighten, A. Weber, R. D. Turner, R. W. Smith, Y. R. Shen, R. Fitzgibbon, B. Lax, C. L. Evans, X. S. Xie, N. Dudovich, D. Yelin, Y. Silberberg, N. Dudovich, D. Yelin, Y. Silberberg, A. G. Caster, S. R. Leone, H. Zhao, M. T. Cicerone, K. A. Marko, L. Rimai, C. Otto, J. Greve, H. Hamaguchi, V. V Yakovlev, M. Bonn, M. Muller, W. Holzapfel, W. Zinth, W. Kaiser, T. Lang, M. Motzkus, S. Roy, T. R. Meyer, J. R. Gord, R. Dasari, M. Feld, J. F. Sperry, J. Reintjes, T. J. Manuccia, G. R. Holton, X. S. Xie, S. Chen and D. D. Dlott, *Science*, 2007, **13**, 268–273.
80 S. B. Kalidindi, H. Oh, M. Hirscher, D. Esken, C. Wiktor, S. Turner, G. Van Tendeloo and R. A. Fischer, *Chem.–Eur. J.*, 2012, **18**, 10848–10856.
81 F. J. Uribe-Romo, J. R. Hunt, H. Furukawa, C. Klöck, M. O'Keeffe and O. M. Yaghi, *J. Am. Chem. Soc.*, 2009, **131**, 4570–4571.
82 R. S. B. Gonçalves, A. B. V. Deoliveira, H. C. Sindra, B. S. Archanjo, M. E. Mendoza, L. S. A. Carneiro, C. D. Buarque and P. M. Esteves, *ChemCatChem*, 2016, **8**, 743–750.
83 C. Xu, J. Lin, D. Yan, Z. Guo, D. J. Austin, H. Zhan, A. Kent and Y. Yue, *ACS Appl. Nano Mater.*, 2020, **3**, 6416–6422.
84 Y. Liu, C. Wu, Q. Sun, F. Hu, Q. Pan, J. Sun, Y. Jin, Z. Li, W. Zhang and Y. Zhao, *CCS Chem.*, 2021, **3**, 2418–2427.
85 Q. Sun, C. Wu, Q. Pan, B. Zhang, Y. Liu, X. Lu, J. Sun, L. Sun and Y. Zhao, *ChemNanoMat*, 2021, **7**, 95–99.
86 I. P. Beletskaya, F. Alonso and V. Tyurin, *Coord. Chem. Rev.*, 2019, **385**, 137–173.
87 A. Taheri Kal Koshvandi, M. M. Heravi and T. Momeni, *Appl. Organomet. Chem.*, 2018, **32**, 1–59.
88 S. E. Hooshmand, B. Heidari, R. Sedghi and R. S. Varma, *Green Chem.*, 2019, **21**, 381–405.